Protonic solid-state electrochemical synapse for physical neural networks

Xiahui Yao [1], Konstantin Klyukin[2], Wenjie Lu[3], Murat Onen[3], Seungchan Ryu[4], Dongha Kim [2], Nicolas Emond [2], Iradwikanari Waluyo[5], Adrian Hunt[5], Jesús A. del Alamo [3✉], Ju Li [1,2✉] & Bilge Yildiz [1,2✉]

Physical neural networks made of analog resistive switching processors are promising platforms for analog computing. State-of-the-art resistive switches rely on either conductive filament formation or phase change. These processes suffer from poor reproducibility or high energy consumption, respectively. Herein, we demonstrate the behavior of an alternative synapse design that relies on a deterministic charge-controlled mechanism, modulated electrochemically in solid-state. The device operates by shuffling the smallest cation, the proton, in a three-terminal configuration. It has a channel of active material, WO_3. A solid proton reservoir layer, PdH_x, also serves as the gate terminal. A proton conducting solid electrolyte separates the channel and the reservoir. By protonation/deprotonation, we modulate the electronic conductivity of the channel over seven orders of magnitude, obtaining a continuum of resistance states. Proton intercalation increases the electronic conductivity of WO_3 by increasing both the carrier density and mobility. This switching mechanism offers low energy dissipation, good reversibility, and high symmetry in programming.

[1] Department of Nuclear Science and Engineering, Massachusetts Institute of Technology, 77 Massachusetts Avenue, Cambridge, MA 02139, USA. [2] Department of Materials Science and Engineering, Massachusetts Institute of Technology, 77 Massachusetts Avenue, Cambridge, MA 02139, USA. [3] Department of Electrical Engineering and Computer Science, Massachusetts Institute of Technology, 77 Massachusetts Avenue, Cambridge, MA 02139, USA. [4] Department of Mechanical Engineering, Massachusetts Institute of Technology, 77 Massachusetts Avenue, Cambridge, MA 02139, USA. [5] National Synchrotron Light Source II, Brookhaven National Laboratory, Upton, NY 11973, USA. ✉email: alamo@mit.edu; liju@mit.edu; byildiz@mit.edu

Deep learning based on neural networks has raised tremendous attention as an approach to accelerate machine learning applications, such as computer vision and natural language processing[1,2]. However, using state-of-the-art GPU/CPU (Graphics Processing Unit/Central Processing Unit) based on CMOS (Complementary Metal–Oxide–Semiconductor) circuits to simulate neural networks requires large memory space and high power consumption[3]. This is limited by the traditional von-Neuman structure of current computer systems, which requires the transfer of large amount of data between memory and CPU[4]. New hardware structures and algorithms, such as in-memory computing, have been proposed to tackle these issues[5–8]. As demonstrated by Jo et al.[9], crossbar-type arrays containing two-terminal resistive switches (or memristors) enable energy-efficient and fast-processing physical neural networks[10–12]. The core component of this physical neural network is the resistive switch, whose electronic conductance can be modulated electrically[8,13,14]. This modulation emulates the strengthening and weakening of synapses in the brain. Capturing this synaptic strengthening or weakening, so-called potentiation or depotentiation behavior, respectively[15], is essential to brain-inspired analog computing, and can accelerate complex computation where precision is less critical[2,16,17]. Arrays of resistive switching units have also been demonstrated for image recognition, for example, of faces and hand-written digits[18,19].

There are two main types of resistive switching mechanisms discussed and used in literature to change the conductance, both of them relying on two-terminal configurations[20]. The conductive-filament (CF) mechanism is based on the formation of a narrowly confined conducting path (made of metal atoms or oxygen vacancies) inside an insulating matrix, typically an insulating oxide[21–24]. The phase-change mechanism (PCM) is realized by changing the material between its conducting and insulating phases, such as the Ge-Sb-Te chalcogenides, controlled by Joule heating[25,26]. Both resistive switching mechanisms have been demonstrated in artificial intelligence applications, but the CF mechanism suffers from lack of reproducibility, while the PCM suffers from high energy dissipation and drift[10,27,28]. As a result, the performance of such two-terminal devices in a memory matrix environment is still far from the desired specifications for reliable, fast and energy-efficient training of neural networks[29]. A fundamentally new working mechanism is desirable for enabling new opportunities to address these challenges.

Recently, three-terminal electrochemical resistive switches demonstrated by Fuller et al. exhibit promising characteristics, in particular multistate capability and low energy consumption[30]. This concept relies on a configuration similar to a Li-ion solid-state battery. LiCoO$_2$ was employed as the switching media, whose conductivity can be modulated by the extent of Li intercalation. Gated by a Si layer and separated from the LiCoO$_2$ channel by a Li$^+$ conducting solid electrolyte, Li$^+$ was pumped into and out of the LiCoO$_2$ active material reversibly. Electrochemical control of Li$^+$ concentration in LiCoO$_2$ enables a large and continuous modulation of electronic resistance. Tang et al. also demonstrated high speed and low power modulation of WO$_3$ channel conductance by Li$^+$ intercalation using 5 ns pulses[31]. The major challenge preventing the scale up of this concept is the utilization of Li as the doping ion. Li is not compatible with current CMOS processing due to its high volatility and manufacturing tool contamination concerns.

Being a smaller and faster diffusing cation than Li$^+$, employing protons (H$^+$) as the doping ion presents potential advantages. The Shannon–Prewitt crystal ionic radius of H$^+$ is −0.04 Å, in contrast to 0.90 Å of Li$^+$. The advantages of using protons include lower energy consumption, higher operation speed, better compatibility with Si technology, and longer

lifetime due to enhanced structural stability of the active material as a result of volume change with successive ion insertion/extraction steps[30–32]. Electrochemical proton shuffling has been implemented by van de Burgt et al.[32] using organic electrode materials, in a three-terminal electrochemical resistive switch configuration. This device demonstrated greater energy efficiency (390 aJ/μm^2) and operating speed (order of ms) than its Li counterpart (~37 nJ/μm^2, order of seconds)[30]. Array-level device demonstrations based on this working mechanism have also been reported, for face recognition and hand-written digit recognition[18,19]. However, the organic nature of the active channel material presents challenges in Si-compatible device fabrication and in long-term stability. While these reports are encouraging, it is desirable to work with a new material system that offers both compatibility with current semiconductor processing protocols and is capable of implementing highly energy efficient analog neural networks. Advancing towards such a technology needs insights from fundamental studies of material atomic and electronic behavior during the resistance modulation process, as well as development of an appropriate gating protocol and device geometry optimization.

In this work, we demonstrate proton intercalation in inorganic materials as a basis for emulating synapse behavior with low energy cost, long retention, and good symmetry. This system offers a deterministic, charged-controlled mechanism that uniformly switches the channel conductance. Thus, it should not pose issues related to lack of reproducibility that heavily depends on the microstructural and chemical heterogeneities in the high-k dielectric materials used in two-terminal CF devices. In addition, if the intercalating ion and the chosen materials are suitable, the energy consumption of the switching process can be very small, as demonstrated in this work. We quantify the protonation-conductance relationship of this artificial electrochemical synapse, providing insights into the proper selection of operating window for the chosen material, WO$_3$. We adopt the constant current gating, and propose that it is more suitable than the constant voltage gating for such three-terminal electrochemical resistive switches because it offers better controllability, reproducibility, and symmetry. X-ray absorption and photoelectron spectroscopy, together with first-principles calculations, reveal that the electronic carrier density and mobility contribute to the conductivity change as a function of protonation in WO$_3$.

Results

Material selection and device configuration. A variety of metal oxides are known to change their electronic conductivity upon cation intercalation, including WO$_3$[17], MoO$_3$[33], VO$_2$[34], and SrCoO$_2$[35]. We chose WO$_3$ as a prototypical proton intercalation host because it is a semiconductor in its undoped state (band gap 2.8~3.2 eV)[36]. We can precisely tune the conductivity by the degree of proton intercalation in this material due to the accompanied filling of electrons into the conduction band[37,38]. With a high concentration of protonation, a tungsten bronze phase (H$_x$WO$_3$) is expected to form that turns the material metallic[31,39,40]. WO$_3$ is also compatible with Si technology[41]. Protonation of such oxides in the past has been demonstrated from gas-phase H$_2$, through an aqueous electrolyte, by hydrolysis of water adsorbed in a porous solid, or through an ionic liquid electrolyte[17,42,43]. Reliance on protonation from gas-phase hydrogen or from water is not conducive to controllable, reversible, and technologically feasible devices. Instead, we use a solid, inorganic and reversible hydrogen reservoir, palladium hydride, PdH$_x$, that is integrated into a three-terminal device as the gate electrode.
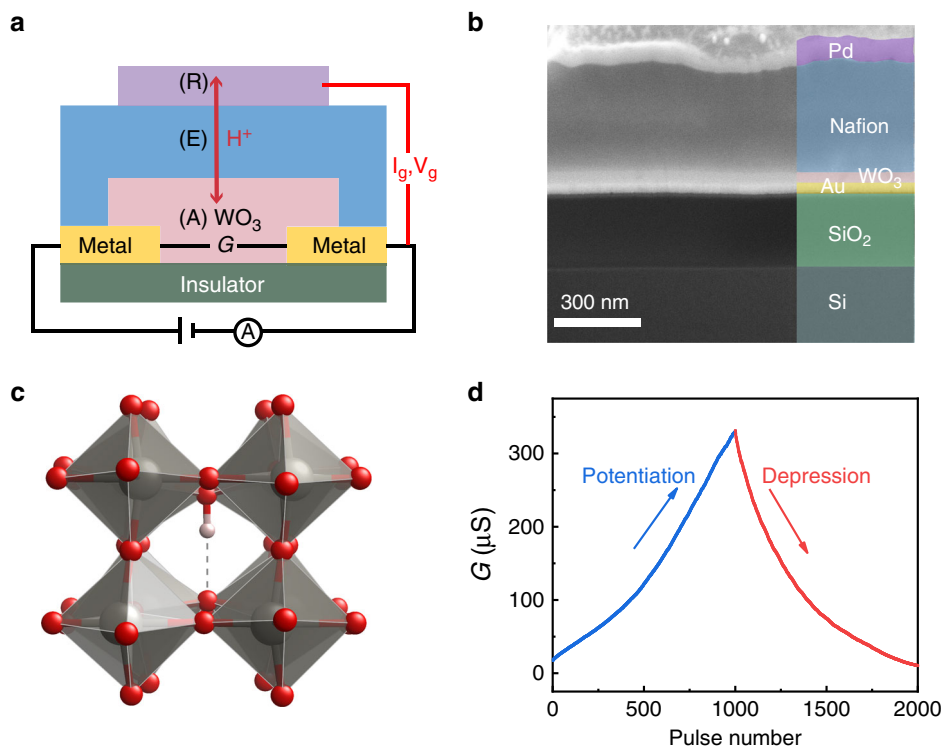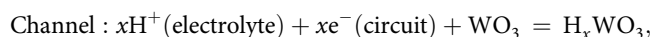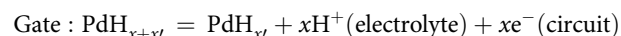
Fig. 1 Device configuration and operating principles. a Schematic of the protonic electrochemical synapse device structure. R: solid-state hydrogen reservoir layer, serving also as gate electrode. E: solid-state proton conductive electrolyte layer. A: active switching layer, serving as conducting channel. G refers to the conductance of the channel between the source and drain electrodes (noted as Metal), calculated from $G = I_d/V_{ds}$, where I_d is the current measured at the drain and V_{ds} is the reading bias applied between the source and drain. I_g, V_{gs}: the gating current and gating voltage, applied between the gate and the source. **b** Scanning electron microscopy image of the device cross-section. **c** WO$_3$ lattice indicating the sites that allow proton intercalation and the bonding between the proton (white sphere) and the oxygen ions (red spheres). The grey spheres are Tungsten atoms. **d** Demonstration of potentiation/depression behavior of the electrochemical synapse by signals of +200 nA/−200 nA and 5 ms; potentiation and depression represent the synaptic strengthening and weakening behavior. Each data point represents the average conductance value of the steady states measured after each gating pulse.

The three-terminal source-drain-gate configuration of the device in this work is shown in Fig. 1a, b. The source and drain electrodes are two gold metal contacts deposited on SiO$_2$ coated Si gapped by a 100 μm long channel. This channel is filled with a 50 nm thick WO$_3$ film by reactive sputtering as the active material. On top of the channel material, a proton-conductive solid-polymer electrolyte (Nafion-117) is deposited by spin coating, resulting in 300–400 nm thickness. This electrolyte layer is electronically insulating but protonically conductive, with the proton conductivity around 0.09 S/cm at room temperature under 100% relative humidity[44]. The gate electrode in this device serves the dual role of reservoir of protons and electrons. Metals with high electronic conductivity and high hydrogen solubility are desirable for this purpose[45]. Palladium metal, which can absorb hydrogen effectively even at room temperature[46], was selected as gate in this demonstration. After the deposition of Pd, hydrogen was introduced to form PdH$_x$ by exposing the device to 5% forming gas at room temperature prior to and during the test.

Operation principles. The conductance between the source and drain electrodes represents the strength of the synapse in a neural network. In this demonstration, a small constant voltage ($V_{ds} = $ +0.1 V) is applied between the source and drain electrodes. The corresponding current signal (I_d) is recorded to calculate the conductance ($G = I_d/V_{ds}$). To modulate the conductance, positive or negative gate current pulses (I_g) are applied to drive protons into or out of the channel material, respectively.

When $I_g > 0$, PdH$_x$ is electrochemically oxidized and releases protons to the Nafion electrolyte. The protons diffuse through the Nafion electrolyte toward the channel oxide, under the driving force of the gating voltage (V_{gs}) between the gate and channel. Once the protons reach the surface of WO$_3$, they intercalate into the WO$_3$ with the simultaneous electron injection from the outer circuit (Supplementary Fig. 1). This process is fully reversible and can be expressed with the following electrochemical reaction:

$$\text{Gate}: \text{PdH}_{x+x\prime} = \text{PdH}_{x\prime} + x\text{H}^+(\text{electrolyte}) + xe^-(\text{circuit})$$

$$\text{Channel}: x\text{H}^+(\text{electrolyte}) + xe^-(\text{circuit}) + \text{WO}_3 = \text{H}_x\text{WO}_3,$$

where e$^-$(circuit) are electrons that are metered and pumped via the outer circuit. The net effect after this positive gate current I_g biasing is the intercalation of hydrogen (proton + electron) into the WO$_3$ channel material. Electrons and protons must enter/exit the channel material simultaneously to maintain global charge neutrality. When the external circuit is cut off (gate is open circuit), the electronic insulating nature of the electrolyte prevents the back flow of electrons, and consequently that of protons too. This retention of protons and electrons in the channel material is key to realizing the nonvolatile nature of this device.

The proton as a small cation could reside in the interconnected channels of the WO$_3$ lattice and bond with the oxygen ion to form OH$_O^{\cdot}$ defect in these channel sites (Fig. 1c). There is a main difference here with respect to the conductive filament (CF) or phase change mechanism (PCM) approach. That is, the intercalation of the protons involves a high degree of spatial
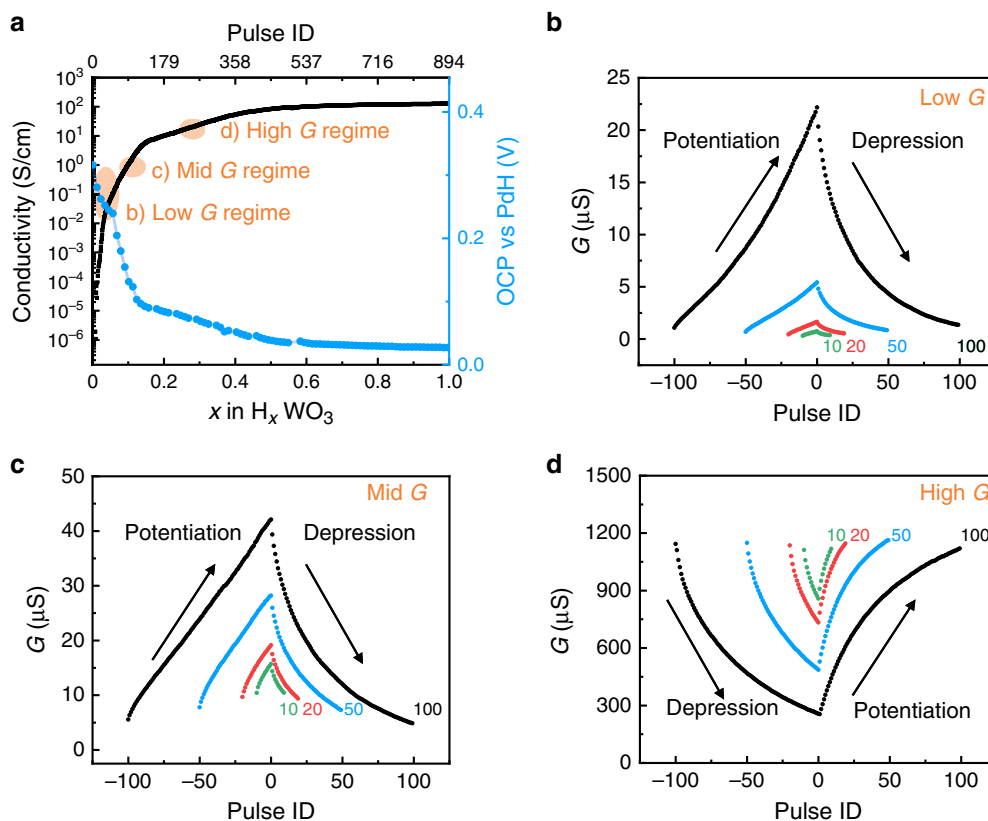
Fig. 2 Range of tunable conductivity, and electrical potentiation in different conductivity regimes. a Dependence of electronic conductivity and open circuit potential (channel WO_3 vs. gate PdH_x) on the hydrogen content in H_xWO_3. **b–d** Reversibility of electronic conductance, and symmetry of potentiation (protonation)–depression (deprotonation) behavior, obtained in the three different protonation regimes starting from (**b**) low conductance regime, (**c**) medium conductance regime and (**d**) high conductance regime (depression first to avoid saturation). 10, 20, 50, and 100 states (upon 10, 20, 50, and 100 pulses, respectively) were obtained for each regime by constant current pulsing for potentiation and depression on the same device. Different conductance regimes were achieved by continuously sending constant current pulses with $0.5\,\mu A$ amplitude and 5 ms width until desired conductance values is reached.

homogeneity within the channel material. This means that the active material (H_xWO_3) can stay single-phase during the intercalation due to the high equilibrium solubility limit of H in the solid solution phase.

As discussed above, and unlike the previous protonation of oxides which rely on the electrolysis of water to generate the protons[47], our device is a closed system with proton shuffling between the solid-state gate and the channel material. This not only reduces the energy consumption by avoiding the water hydrolysis reaction, but also improves the controllability. In a practical device, this electrochemical synapse should be encapsulated by insulating layers that are also proton barriers in order to prevent the long-term loss of protons or ingress of oxygen into the system, essential for device endurance. (See Supplementary Figs. 6 and 14 for demonstration of the encapsulated device).

Electrical response. The full range of the conductivity dependence on the hydrogen concentration in WO_3 (H_xWO_3) that is measured in our device is shown in Fig. 2a. A potentiation pulse train was applied to the device with constant current ($0.5\,\mu A$) and fixed width (5 ms) for each pulse. Between two pulses, the gating circuit was at open circuit for 1 s, during which both the channel conductance (G) and the open circuit potential (OCP, between the gate and channel) were measured. With this process, we increased the H content (x) from nominally 0 as in WO_3 (W^{6+}) to the theoretical maximum of 1 as in HWO_3 (W^{5+}). The H

content (x) was estimated from the net charge transferred by the gate, which was evaluated by integrating the gate current over the pulse time and assuming 100% Coulombic efficiency. As demonstrated in Fig. 2a, over seven orders of magnitude change in conductivity was achieved across the full protonation range.

The slope of conductivity vs. x is not a constant across the full range. When the conductivity is plotted in log scale, as done in Fig. 2a, there are clear changes in the slope at $x = 0.03$, 0.15, and 0.5. We ascribe these to the boundaries between three different regimes of protonation, that correspond to a low conductance regime, a medium conductance regime, and a high conductance regime. These are designated as Low G, Mid G and High G, respectively, on Fig. 2a. The dependence of the conductance slope on the hydrogen concentration implies different conduction mechanisms. This can arise from factors such as defect–defect interactions as the proton concentration increases, or crystal structure change. The slope of the OCP also changes as a function of protonation regime, as seen in Fig. 2a. This implies the involvement of phase change as transitioning from one regime to another (Supplementary Discussion 3 in Supplementary Information).

The electrical response of the device, including the ratio of the maximum to minimum conductance achieved (G_{max}/G_{min}) and the symmetry of potentiation–depression, depend on the degree of protonation in WO_3, or the corresponding conductivity regime, as shown in more detail in Fig. 2b–d. The low hydrogen content (low conductance, Fig. 2b) regime offers better symmetry and higher G_{max}/G_{min} ratio. The high hydrogen content (high conductance) regime features larger changes in the absolute

conductivity per pulse (per the same amount of change in the H quantity) at the cost of poor symmetry. These results guide the choice of an operating window for the device that depends on the performance matrix that is most desirable.

To demonstrate reversibility, constant current pulse trains containing different polarity but the same amplitude (0.5 μA) and width (5 ms) were applied between the gate and the channel. When the protonation of WO_3 is confined to the low conductance regime shown in Fig. 2b, after 100 positive gating pulses, the conductance of the channel increased from 1 μS to 22 μS, demonstrating a continuum of 100 states and a G_{max}/G_{min} ratio of more than 22 (black trace). Upon the application of an identical but negative current pulse train, the conductance decreased to the original low state, accomplishing the depression process. The number of states achieved during this process can be tuned with different number of pulses, and with the pulse height–width that control the degree of protonation in each operation. The states need to be distinguishable from each other by the electronic resistance measurement apparatus. Based on the current device and experimental set up, we have demonstrated 1000 states, with an average $\Delta G/G$ of 0.3% per pulse and an overall G_{max}/G_{min} of 30, as shown in Fig. 1d. These values are in line with the desirable specifications of resistive processing units as assessed by Gokmen et al.[29], and can be further improved with optimization of device geometry and electronic measurement sensitivity. The G_{max}/G_{min} ratio also depends on the pulse number, being 2, 4, 8, and 22, for the 10 (Green), 20 (Red), 50 (Blue) and 100 (Black) pulses, respectively, in the low-G regime as shown in Fig. 2b.

An identical procedure in the medium and high conductance regimes (higher H content) gives smaller G_{max}/G_{min} ratios, as shown in Fig. 2c, d, respectively. Taking the switching behavior of 100 pulses as an example, the three regimes denoted as Low G, Mid G, and High G result in distinctly different G_{max}/G_{min} ratio of 22, 8, and 4, respectively. In addition, a less symmetrical shape was observed in the higher conductance regime. Comparing the 10, 20, 50, and 100 pulse behavior in either protonation regime, a shallower protonation/deprotonation in WO_3 allows better reversibility (the potentiation/depression symmetry). But this comes at the expense of a smaller conductance G_{max}/G_{min} ratio. When compared with the symmetry behavior in prior demonstrations of the two-terminal conductive filament resistive switches[9,48], a significant improvement of symmetry is observed here.

There is still a small extent of hysteresis in our potentiation–depression data. This originates from the long time scale of the equilibration of the protonated state due to proton diffusion from the Nafion-WO_3 interface to the bulk of WO_3 layer (and vice versa). With the same sampling period applied to all measurements, we had to acquire the non-equilibrated states at higher H content regimes which took longer time to equilibrate. Reducing the channel layer thickness (smaller diffusion length) and reducing the pulse width and height (smaller amount of H exchange per pulse) will help to accelerate the kinetics of relaxation and improve the symmetry further. As seen in Fig. 1d, when the pulse amplitude is 200 nA, the inserted hydrogen amount during each pulse is less, and the equilibration is faster, thus giving a more symmetric potentiation/depression behavior even with 1000 pulses, compared with the behavior in Fig. 2 obtained by 0.5 μA pulse amplitude.

The average voltage resulting from the gating pulses is shown in Fig. 3a. With the pulse current of ±0.5 μA, the resulting gate voltage in each potentiation step, V_{gs} is smaller than ±0.5 V. The energy consumption per unit change in conductance, ΔG, during the gating process can be estimated by the integration of the charge vs. voltage. With the average gating voltage of 0.25 V resulting from current pulses of 0.5 μA and 5 ms, an average ΔG

of 48 nS, and an area of $0.6 \times 1.2 \text{ mm}^2$, the average energy cost per unit area per unit conductance change is only 18 aJ/(μm² × nS). This value is significantly smaller than the energy consumption of the conductive filament or phase change mechanisms, and similar to that of state-of-the-art protonic organic devices recorded in the literature[32].

The low operating voltage of <0.5 V also proves that we do not rely on the water electrolysis to supply the protons. To electrolyze water, a minimum of 1.23 V is necessary to meet the thermodynamic requirement and an additional 0.5–0.7 V is needed to break the kinetic overpotential[49], even on the best electrocatalysts. So, we can confidently rule out the possibility of water electrolysis here.

Two features of this protonic electrochemical synapse discussed here enable this low operating energy. First, the cation employed here to modulate the conductivity is the smallest and lightest cation, the proton, needing low energy to migrate and transfer at interfaces. Second, the electrochemical potentials of the gate and channel materials are close, resulting in a small open-circuit potential, as shown in Fig. 2a. This means that the device is operated only within a small voltage window. The first feature minimizes the kinetic contribution to the energy consumption, while the second one minimizes the thermodynamic contribution. In addition, the small but non-zero open-circuit potential change after gating indicates that a selector component may be needed to program individual synapses in an array, as demonstrated in ref. [19], and to avoid cross-talk of individual synapses when not gating.

To demonstrate the endurance of the device, a repeated potentiation and depression cycling test was performed and shown in Fig. 3b. Each cycle contains 100 potentiation and 100 depression pulses. This process was repeated 100 times. The G_{max}/G_{min} ratio remained consistent around 3 across the 100 cycles, demonstrating a device endurance >20,000 pulses. Additional endurance tests at different conductivity regimes, number of states, and encapsulation of the device are provided in Supplementary Figs. 3–6. Potential failure mode of this type of device are the ingression of oxygen, out diffusion of hydrogen, <100% Faradic efficiency, and electrode degradation. Each of these modes of failure can be overcome by proper encapsulation, that warrants future work. (See Supplementary Discussion 2).

Resistance modulation mechanism. To probe how protonation changes the electronic structure of WO_3, we investigated its valence band structure by X-ray photoelectron spectroscopy (XPS). Before proton intercalation, the valence band of pristine WO_3 features a broad peak located around 7 eV below the Fermi level (Fig. 4a)[37]. The extrapolation of the upper edge of this band leads to a valence band maximum located ~2.5 eV below the Fermi level (binding energy = 0 eV) and the photoelectron emission is nearly zero at the Fermi level. This measurement confirms the semi-conductive nature of unprotonated WO_3, with the Fermi level positioned within the band gap. After proton intercalation (~$H_{0.08}WO_3$, see details in Supplementary Figs 7–8 for sample configuration used in X-ray spectroscopy experiments), a new prominent peak appears at nearly 0.5 eV below the Fermi level, indicating the filling of electrons in W $5d(t_{2g})$. The photoelectron emission is also non-zero at the Fermi level. These two observations indicate the filling of electrons into the previously empty conduction band and transition to a metallic conduction mechanism[4].

The oxidation state of W was probed by the W $4f$ photoelectron peaks in Fig. 4b. For the unprotonated WO_3, the binding energy of the of W $4f_{7/2}$ and W $4f_{5/2}$ peaks are located at 35.9 eV and 38.0 eV, respectively. This spectrum is consistent
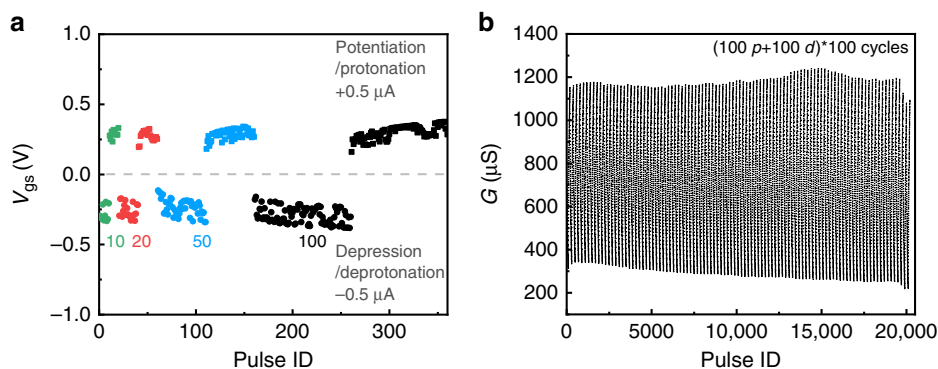
Fig. 3 Gate voltage resulting from gate current pulses, and retention of multistate capability upon cycling. a Average potentiation/depression voltage, resulting from pulses of ±0.5 µA and 5 ms, during the operation of the device in the medium conductance regime shown in Fig. 2c. **b** The retention of multi state capability over 100 cycles of the device, each cycle contains 100 potentiation and 100 depression steps. These data are obtained in the high conductivity regime.
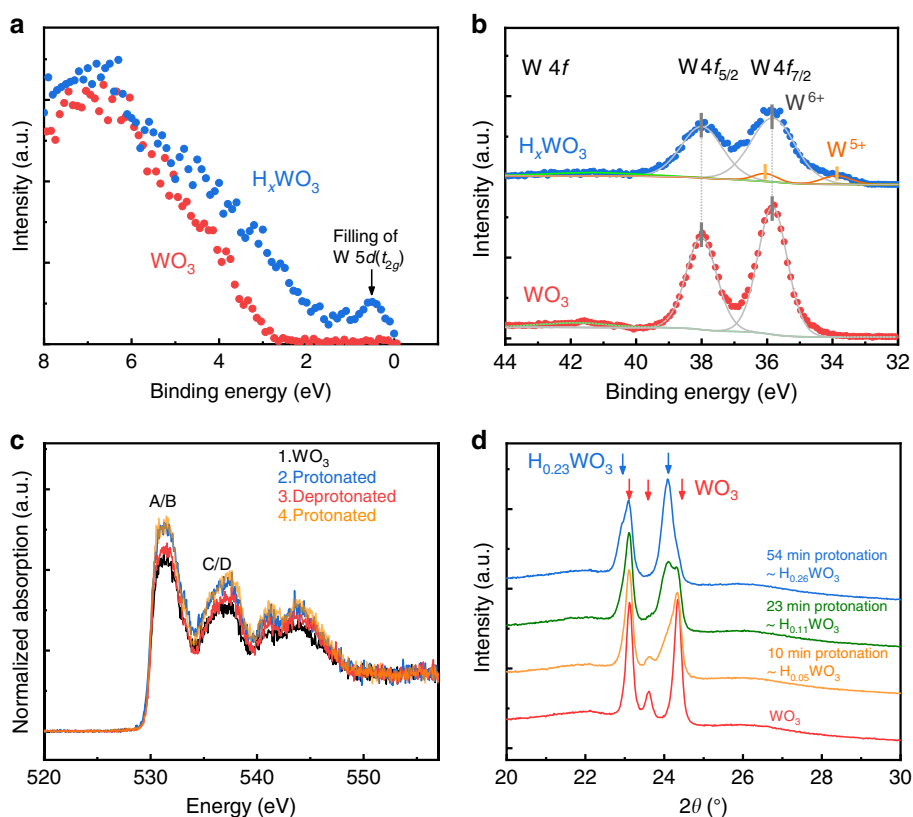

Fig. 4 Electronic and crystallographic structure during protonation to tune the conductance. a Intensity of photoelectron emission vs. binding energy, at the low binding energy region corresponding to the valence band of WO_3 and protonated H_xWO_3, measured by X-ray photoelectron spectroscopy (XPS). **b** W $4f$ photoelectron emission peak, measured by XPS. The oxidation states of WO_3 and protonated H_xWO_3 were deduced from the position of the W $4f_{7/2}$ peak. **c** X-ray absorption spectra of the oxygen K-edge, upon two cycles of protonation/deprotonation: (1) WO_3, (2) first cycle protonated H_xWO_3, (3) deprotonated WO_3, and (4) second cycle protonated H_xWO_3. **d** Crystal structure change probed by X-ray diffraction pattern with heavy proton intercalation corresponding to the different conduction regimes shown in Fig. 2a.

with W^{6+} [50]. After protonation, a new W $4f_{7/2}$ component at 33.8 eV was identified. This lower binding energy corresponds to the reduced W oxidation state of 5+ [51]. Deconvolution of the peaks reveals the ratio between W^{5+} and W^{6+} to be 1:11.4, corresponding to $H_{0.08}WO_3$.

From the analysis of the valence band and the W $4f$ photoelectron peak, we can conclude that, upon intercalation of protons, new in-gap states form, gradually lowering the effective bandgap of WO_3 to 0. This process is accompanied by the injection of electrons, which pushes the Fermi level toward the

conduction band. When the quantity of injected electrons is significant enough, the Fermi level completely shifts into the conduction band. Consistent with electron injection and n-type doping, the oxidation state of W is reduced. As a result, we expect a continuous increase of electronic conductivity with increasing protonation level in H_xWO_3, as shown in Fig. 2a.

In addition to the increase in carrier density, the protonation of WO_3 could result in an increase in the mobility of the electronic charge carriers, that may arise from the increase in hybridization of W–O bonds. In operando X-ray absorption spectroscopy of the

O K-edge region measured during the protonation of WO_3 provides strong evidence for this effect. The O K-edge spectra of WO_3 prior to and after protonation is shown in Fig. 4c (see sample configuration in Supplementary Fig. 7). A prominent absorption peak denoted as A/B at the photon energy of c.a. 530 eV corresponds to electron excitation from core level O 1s to the empty states in O 2p, which is created by W $5d(t_{2g})$-O 2p hybridization[52,53]. The intensity of this peak is positively correlated with the hybridization level (covalency) of the W–O bonds[54]. After protonation (Trace 2, blue), the A/B peak intensity increases compared with the state prior to protonation (Trace 1, black). This indicates a higher level of hybridization after protonation. Because this hybridization is featured by electron donation from the O 2p orbital in the valence band to the W 5d (t_{2g}) orbital in the conduction band, the increased hybridization results in a larger extent of electron delocalization[55], which is usually accompanied by higher electron mobility[56]. In addition, the peaks at c.a. 535–537 eV (C/D) reflect the hybridization of the W $5d(e_g)$-O 2p states, and these peaks are sensitive to the O 2p-H 1s interaction[52]. The increase of intensity in C/D peaks after protonation is a direct evidence of proton intercalation into WO_3. The observed changes in the O K-edge are reversible upon cycling between protonation and deprotonation. The peak intensities of the A/B and C/D regions decrease with deprotonation (Trace 3, red), and increase again with a subsequent protonation (Trace 4, orange) (Supplementary Fig. 8 for details). This modulation of the degree of W $5d(t_{2g})$-O 2p hybridization changes the extent of electron delocalization, and thus, the electron mobility.

First-principles calculations of electronic structure also give evidence to the increase of charge carrier density and mobility upon increased protonation in WO_3[38]. The evolution of the electronic structure in monoclinic H_xWO_3 upon hydrogenation ($x = 0–0.125$) is shown in Fig. 5. The calculated direct band gap of pure monoclinic WO_3 is 2.82 eV, in good agreement with the available experimental data[36] and Supplementary Fig. 9. As it is seen from Fig. 5b, the conduction band of monoclinic WO_3 is mainly composed of unoccupied W 5d orbitals, while O 2p orbitals dominate in the valence band region.

Insertion of protons at the channel sites as shown in Fig. 1c, followed by subsequent charge balancing leads to the formation of in-gap states (Fig. 5d), at 0.28 eV below the conduction band for $x = 0.0156$. At low hydrogen concentrations, the excess electrons are localized over several adjacent W atoms located in the same plane forming a large 2D polaron with a radius of ≥15 Å, as shown in Fig. 5c.

With increasing protonation, the localized in-gap states monotonically approach the conduction band minima, decreasing the ionization energy from 0.28 eV at $x = 0.0156$ to 0.08 eV at $x = 0.0625$. Further protonation up to $x = 0.125$ leads to a metallic behavior of $H_{0.125}WO_3$, as shown in Fig. 5e, f. The computed changes in electronic structure correlate well with the decreased oxidation state of W and the disappearance of the band gap at $x = 0.08$ probed by XPS shown in Fig. 4a–c.

At higher protonation levels ($x > 0.1$), the distortion of the lattice may actually change the crystal structure[57], and thus, its band structure. To study this, we performed in operando X-ray diffraction to study the structure evolution. Prior to protonation, WO_3 exhibits the most stable monoclinic structure[57], as shown by the red pattern denoted as WO_3 in Fig. 4d, with three major diffraction peaks at 23.1°, 23.6°, and 24.3°. They correspond to the (002), (020), and (200) planes (JCPDS 83-0950). During continuous biasing with $I_g = +1 \mu A$, the (002) and (200) peaks of WO_3 shifted toward lower angles after 10 min ($x = 0.05$). After 54 min of biasing ($x = 0.26$ by assuming 100% Coulombic efficiency, see Supplementary Table 1), these two peaks eventually shift to 22.9° and 24.1°, corresponding to +1.29% and 0.95% lattice expansion, respectively. These two peaks can be related to the (001) and (110) planes of the tetragonal $H_{0.23}WO_3$ (JCPDS 85-0967, Supplementary Fig. 8 for higher angle XRD data). The original (020) peak of monoclinic WO_3 at 23.6° disappeared during the process because of increased symmetry. The total unit cell volume expanded only a very small amount, +0.28% for 0.23
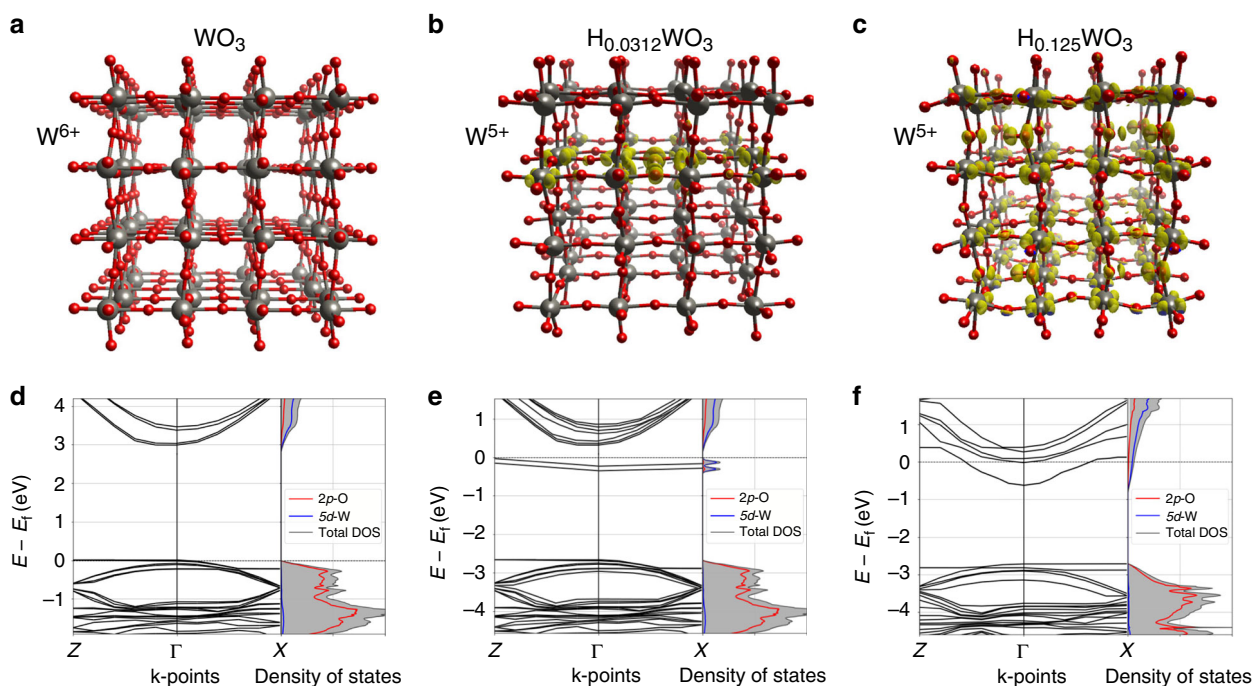

Fig. 5 Calculated electronic structure with protonation in WO_3. Crystal structures, charge density maps and corresponding electronic band structure and density of states for (**a**, **b**) WO_3, (**c**, **d**) $H_{0.0312}WO_3$, (**e**, **f**) $H_{0.125}WO_3$; grey atoms—W, red—O and white—H. The excess charge associated with the H insertion is shown in yellow (isosurface – 0.04 e/Å³).

H per unit WO_3. For comparison, the c-axis change from Li_0CoO_2 to $Li_{0.25}CoO_2$ is nearly 9.3%[58]. The reduction of lattice stress further highlights the advantage of H^+ over Li^+ in terms of structural stability[59].

As a result of this in situ XRD analysis, we can conclude that, with the insertion of protons into the channel sites, the WO_6 octahedra become more ordered and the crystal structure becomes more symmetrical, as seen from the monoclinic to tetragonal transition in Fig. 4d. The increased symmetry can arise from increased concentration of electronic charge in WO_3, namely W^{5+}/W^{6+} polarons. We have also found that the interaxial angles approach 90° upon proton insertion in WO_3 (see Supplementary Fig. 11 in Supplementary Information.) The increased symmetry of the structure can also contribute to a change of the band structure[60] and eventually the conductive behavior[39,57].

Gating strategy of electrochemical synapses. Gating through the application of a voltage is widely adopted in the literature to induce resistive switching (also demonstrated in Supplementary Fig. 12 on our device)[61]. Typical reported gating voltage values range from several volts to tens of volts. Very often, the gating voltage is used as a descriptor to indicate the final state of the sample[49,62]. Here we emphasize that, in such an electrochemical synapse (or ionic gating) devices, there can be a significant difference between the gating voltage applied and the change in the open-circuit potential of the device due to polarization. That is, the equilibrium chemical potential of the active material does not necessarily follow the applied gating voltage precisely[63]. Such difference could be a major reason for the lack of consistency of the gating voltages reported in the literature[17,40,49,64].

There are two major points to consider. First, the voltage applied during the ionic gating is spent on several contributions; the chemical potential difference between the gate and the channel electrodes, ionic ohmic loss across the electrolyte, and the Nernst overpotential to drive the electron-ion exchange at the electrode–electrolyte interface. The steady-state chemical potential of the active material achieved after the constant voltage gating represents only the first part, and the latter two are the kinetic loss terms.

Second, even if the correlation between the gating voltage and the chemical potential at the electrode–electrolyte interface can be properly established, the time needed to reach equilibrium within the bulk of the channel material is non-negligible. This is due to the finite diffusion time of ions in solids (Supplementary Fig. 13).

Based on these considerations, we propose two directions to evade the issue related to voltage gating. First, as adopted in this paper, constant current gating, rather than constant voltage gating, should provide a deterministic switching behavior, by using the accumulated charge as the descriptor for the status of the channel. Second, employing cations with high diffusivity, such as the proton, and reducing the thickness of the channel layer, should minimize the diffusion time and the resulting time-dependent relaxation of the channel conductance.

In summary, we have designed and demonstrated a protonic electrochemical synapse as an all-solid-state device, with very low energy consumption (18 aJ/($\mu m^2 \times nS$)), nearly symmetrical potentiation (protonation)/depotentiation (deprotonation) behavior, long cycling lifetime, and featuring small changes in OCP. The core material system comprising WO_3 as the channel and PdH_x as the gate electrode (solid proton reservoir), were chosen in order to be CMOS compatible. In the complete range from 0 to 1 H per WO_3, we achieved continuous modulation of the conductance and a high G_{max}/G_{min} ratio of 10^7. The lower protonation regime features higher potentiation/depotentiation

symmetry. The higher protonation regime features small OCP change and large ΔG per unit amount of proton insertion. This understanding provides guidance for selection of an operating window to achieve desired device properties. In addition, we confirmed the topotactic nature of the conductivity modulation of our device through electronic and atomic structure analysis, with the observed volume change much smaller than Li-intercalation compounds, thus promising smaller residual stress and longer cycle life. The inorganic protonic electrochemical synapse demonstrated here, and the understanding generated from this study, provide a path to low-energy and reliable artificial synapses as hardware for artificial neural networks that are capable of accelerating artificial intelligence development.

Methods

Device fabrication. The device adopted a three-terminal thin-film transistor configuration. The source and drain electrodes composed of 40 nm thick Au was deposited by RF sputtering. A channel with a width of 500 μm and length of 100 μm between the source and drain electrodes was patterned by shadow mask. This channel was further filled by 50 nm thick WO_3, which was deposited by reactive RF sputtering from W metal target with the Ar:O_2 ratio of 9.3:2.7 at 3 mtorr. The deposited film was further annealed at 450 °C for 1 h in air to achieve crystalized monoclinic WO_3 phase. Spin coating was employed to apply Nafion-117 resin solution (Sigma-Aldrich) on top of WO_3 as solid proton conductor layer. The thickness of the proton electrolyte layer can be adjusted by the spin speed and concentration to achieve 300–400 nm in thickness. After drying the Nafion layer in ambient air followed by 100 °C baking, the device was transferred back to the sputtering chamber for Pd top gate electrode deposition patterned by shadow mask.

Electrical measurements. The as-fabricated device was transferred into a moisturized chamber filled with 5% hydrogen in argon atmosphere and nearly 100% relative humidity at room temperature. The hydrogen absorption by Pd can be observed by continuous open circuit measurement of WO_3 (channel) vs. Pd (Gate), which changes from negative to positive, due to the electrochemical potential change when Pd is converted into PdH_x. The electrical test was performed inside the chamber without exposing to the ambient air. A constant voltage of +100 mV was applied between the source and drain, the corresponding current (I_d) was recorded by Keithley 2460 to calculate the conductance level. A constant current pulse train with ±0.5 μA amplitude, 5 ms width and 1 s interval were applied by Gamry reference 3000 potentiostat or Keithley 2400 source meter to the gate to induce the potentiation and depression characteristic behavior of resistive switching. The gate voltage was recorded every 1 ms during the pulse to calculate the energy consumption per pulse. Between pulses, the gate electrode was set at open circuit condition (high impedance mode) for OCP measurement for 1 s.

Material characterization. X-ray diffraction pattern was collected on Rigaku Smartlab diffractometer (Cu Kα λ = 1.5406 Å) in situ. A device with the same configuration as described above but with larger size (WO_3 pad: 8.3 mm × 5 mm × 100 nm) was prepared for this test to ensure the intensity of diffraction signal to be strong enough. The device was encapsulated in a sample holder with X-ray transparent windows made by Mylar film. The chamber was filled with 5% H_2 in Argon and the electric bias was applied by Keithley 2460.

The ambient pressure soft XAS data was collected at the 23-ID-2 (IOS) beamline at the National Synchrotron Light Source II (NSLS-II) at Brookhaven National Laboratory. Partial fluorescence yield signal, measured using a Vortex EM silicon drift detector, was chosen as the signal to be collected due to its relatively large probing depth (~100 nm). With this probing depth, we consider the data collected to be sensitive to the bulk of film, given that our film is typically 50 nm thick. Detection area was carefully chosen at the edge of the WO_3-Au interface (See Supplementary Fig. 7). The device was first transferred into the in operando ambient pressure XAS chamber, after which 5 mTorr H_2O and 400 mTorr H_2 was introduced into the chamber. A reference spectrum was collected without external bias, and denoted as WO_3 in Fig. 4c. A continuous negative current was further applied on the WO_3 through the Au contact. It is expected that hydrogen will split into hydrogen atom on the Pd side, which can be electrochemically pumped into WO_3 through the electrolyte, even under such low hydrogen partial pressure.

The XPS measurement and valence band measurement were collected by PHI Versaprobe II spectrometer with Al Kα source. XPS measurement was taken ex situ for the same sample after XAS measurement at the protonated state.

The cross-sectional samples were prepared by FEI Helios Nanolab 600 focused ion beam system and imaged in the same instrument by electron beam.

Density functional theory calculations. First-principles calculations were performed within the density functional theory formalism using the projector augmented wave potentials[65] as implemented in the Vienna Ab initio Simulation

Package [66]. The screened Heyd-Scuseria-Ernzerhof hybrid functional for solids[67] was employed to accurately describe many-electron interactions, charge localization, and lattice parameters The calculation were performed for monoclinic WO_3 (space group P21/n) supercell of 14.70 Å × 15.01 Å × 15.41 Å (β = 90.17°) with multiple H atoms to simulate the concentration range of $x = 0$–0.125. A mesh of $4 \times 4 \times 4$ **k**-points and a 500 eV cut-off energy were employed for supercell calculations.

Data availability
The data that support the findings of this study are available from the corresponding authors upon request.

References
1. Essera, S. K. et al. Convolutional networks for fast energy-efficient neuromorphic computing. *Proc. Natl Acad. Sci. U. S. A.* **113**, 11441–11446 (2016).
2. Tang, J. et al. Bridging biological and artificial neural networks with emerging neuromorphic devices: fundamentals, progress, and challenges. *Adv. Mater.* **31**, 1902761 (2019).
3. Suleiman, A., Chen, Y., Emer, J. & Sze, V. in *2017 IEEE International Symposium on Circuits and Systems (ISCAS)*. 1–4 (IEEE, 2017).
4. Sebastian, A. et al. Temporal correlation detection using computational phase-change memory. *Nat. Commun.* **8**, 1115 (2017).
5. Wong, H. S. P. & Salahuddin, S. Memory leads the way to better computing. *Nat. Nanotech.* **10**, 191–194 (2015).
6. Ambrogio, S. et al. Equivalent-accuracy accelerated neural-network training using analogue memory. *Nature* **558**, 60–67 (2018).
7. Burr, G. W. et al. Neuromorphic computing using non-volatile memory. *Adv. Phys.* **2**, 89–124 (2017).
8. Ielmini, D. & Wong, H. S. P. In-memory computing with resistive switching devices. *Nat. Electron.* **1**, 333–343 (2018).
9. Jo, S. H. et al. Nanoscale memristor device as synapse in neuromorphic systems. *Nano Lett.* **10**, 1297–1301 (2010).
10. Yang, J. J. S., Strukov, D. B. & Stewart, D. R. Memristive devices for computing. *Nat. Nanotech* **8**, 13–24 (2013).
11. Sheridan, P. M. et al. Sparse coding with memristor networks. *Nat. Nanotech.* **12**, 784–789 (2017).
12. Wang, Z. et al. Capacitive neural network with neuro-transistors. *Nat. Commun.* **9**, 3208 (2018).
13. Strukov, D. B., Snider, G. S., Stewart, D. R. & Williams, R. S. The missing memristor found. *Nature* **453**, 80–83 (2008).
14. Linn, E., Rosezin, R., Kügeler, C. & Waser, R. Complementary resistive switches for passive nanocrossbar memories. *Nat. Mater.* **9**, 403–406 (2010).
15. Ohno, T. et al. Short-term plasticity and long-term potentiation mimicked in single inorganic synapses. *Nat. Mater.* **10**, 591–595 (2011).
16. Haensch, W., Gokmen, T. & Puri, R. The next generation of deep learning hardware: analog computing. *P. IEEE* **107**, 108–122 (2019).
17. Yang, J.-T. et al. Artificial synapses emulated by an electrolyte-gated tungsten-oxide transistor. *Adv. Mater.* **30**, 1801548 (2018).
18. Liu, Q. et al. Fully printed all-solid-state organic flexible artificial synapse for neuromorphic computing. *ACS Appl. Mater. Interfaces* **11**, 16749–16757 (2019).
19. Fuller, E. J. et al. Parallel programming of an ionic floating-gate memory array for scalable neuromorphic computing. *Science* **364**, 570–574 (2019).
20. Wouters, D. J., Waser, R. & Wuttig, M. Phase-change and redox-based resistive switching memories. *P. IEEE* **103**, 1274–1288 (2015).
21. Waser, R. & Aono, M. Nanoionics-based resistive switching memories. *Nat. Mater.* **6**, 833–840 (2007).
22. Du, H. C. et al. Nanosized conducting filaments formed by atomic-scale defects in redox-based resistive switching memories. *Chem. Mater.* **29**, 3164–3173 (2017).
23. Lanza, M. et al. Recommended methods to study resistive switching devices. *Adv. Electron. Mater.* **5**, 1800143 (2019).
24. Wang, Z. et al. Memristors with diffusive dynamics as synaptic emulators for neuromorphic computing. *Nat. Mater.* **16**, 101–108 (2017).
25. Zhang, W., Mazzarello, R., Wuttig, M. & Ma, E. Designing crystallization in phase-change materials for universal memory and neuro-inspired computing. *Nat. Rev. Mater.* **4**, 150–168 (2019).
26. Kuzum, D., Jeyasingh, R. G., Lee, B. & Wong, H.-S. P. Nanoelectronic programmable synapses based on phase change materials for brain-inspired computing. *Nano Lett.* **12**, 2179–2186 (2011).
27. Ielmini, D. Resistive switching memories based on metal oxides: mechanisms, reliability and scaling. *Semicond. Sci. Technol.* **31**, 063002 (2016).
28. Waser, R., Dittmann, R., Staikov, G. & Szot, K. Redox-based resistive switching memories - nanoionic mechanisms, prospects, and challenges. *Adv. Mater.* **21**, 2632–2663 (2009).
29. Gokmen, T. & Vlasov, Y. Acceleration of deep neural network training with resistive cross-point devices: design considerations. *Front. Neurosci.* **10**, 333 (2016).
30. Fuller, E. J. et al. Li-Ion synaptic transistor for low power analog computing. *Adv. Mater.* **29**, 1604310 (2017).
31. Tang, J. et al. in *2018 IEEE International Electron Devices Meeting (IEDM)*. 13.11.11–13.11.14 (IEEE, 2018).
32. van de Burgt, Y. et al. A non-volatile organic electrochemical device as a low-voltage artificial synapse for neuromorphic computing. *Nat. Mater.* **16**, 414–418 (2017).
33. Julien, C. & Nazri, G. A. Transport properties of lithium-intercalated MoO_3. *Solid State Ion.* **68**, 111–116 (1994).
34. Yoon, H. et al. Reversible phase modulation and hydrogen storage in multivalent VO_2 epitaxial thin films. *Nat. Mater.* **15**, 1113–1119 (2016).
35. Lu, N. et al. Electric-field control of tri-state phase transformation with a selective dual-ion switch. *Nature* **546**, 124–128 (2017).
36. Vemuri, R. S., Engelhard, M. H. & Ramana, C. V. Correlation between Surface Chemistry, Density, and Band Gap in Nanocrystalline WO_3 Thin Films. *ACS Appl. Mater. Interfaces* **4**, 1371–1377 (2012).
37. Niklasson, G. A. & Granqvist, C. G. Electrochromics for smart windows: thin films of tungsten oxide and nickel oxide, and devices based on these. *J. Mater. Chem.* **17**, 127–156 (2007).
38. Hjelm, A., Granqvist, C. G. & Wills, J. M. Electronic structure and optical properties of WO_3, $LiWO_3$, $NaWO_3$, and HWO_3. *Phys. Rev. B* **54**, 2436–2445 (1996).
39. Kamal, H., Akl, A. A. & Abdel-Hady, K. Influence of proton insertion on the conductivity, structural and optical properties of amorphous and crystalline electrochromic WO_3 films. *Phys. B* **349**, 192–205 (2004).
40. Leng, X. et al. Insulator to metal transition in WO_3 induced by electrolyte gating. *npj Quantum Mater.* **2**, 35 (2017).
41. Cai, F. et al. A fully integrated reprogrammable memristor–CMOS system for efficient multiply–accumulate operations. *Nat. Electron.* **2**, 290–299 (2019).
42. Nishihaya, S. et al. Evolution of insulator–metal phase transitions in epitaxial tungsten oxide films during electrolyte-gating. *ACS Appl. Mater. Interfaces* **8**, 22330–22336 (2016).
43. Altendorf, S. G. et al. Facet-independent electric-field-induced volume metallization of tungsten trioxide films. *Adv. Mater.* **28**, 5284–5292 (2016).
44. Sone, Y., Ekdunge, P. & Simonsson, D. Proton Conductivity of Nafion 117 as Measured by a Four-Electrode AC Impedance Method. *J. Electrochem. Soc.* **143**, 1254–1259 (1996).
45. Rusman, N. A. A. & Dahari, M. A review on the current progress of metal hydrides material for solid-state hydrogen storage applications. *Int. J. Hydrog. Energy* **41**, 12108–12126 (2016).
46. Li, Y. & Cheng, Y.-T. Hydrogen diffusion and solubility in palladium thin films. *Int. J. Hydrog. Energy* **21**, 281–291 (1996).
47. Zhu, L. Q., Wan, C. J., Guo, L. Q., Shi, Y. & Wan, Q. Artificial synapse network on inorganic proton conductor for neuromorphic systems. *Nat. Commun.* **5**, 3158 (2014).
48. Jiang, H. et al. Sub-10 nm Ta channel responsible for superior performance of a HfO_2 memristor. *Sci. Rep.* **6**, 28525 (2016).
49. Katase, T., Onozato, T., Hirono, M., Mizuno, T. & Ohta, H. A transparent electrochromic metal-insulator switching device with three-terminal transistor geometry. *Sci. Rep.* **6**, 25819 (2016).
50. Katrib, A., Hemming, F., Wehrer, P., Hilaire, L. & Maire, G. The multi-surface structure and catalytic properties of partially reduced WO_3, WO_2 and WC + O_2 or W + O_2 as characterized by XPS. *J. Electron Spectrosc. Relat. Phenom.* **76**, 195–200 (1995).
51. ViolBarbosa, C. et al. Transparent conducting oxide induced by liquid electrolyte gating. *Proc. Natl Acad. Sci. U. S. A.* **113**, 11148–11151 (2016).
52. Purans, J., Kuzmin, A., Parent, P. & Laffon, C. Study of the electronic structure of rhenium and tungsten oxides on the O K-edge. *Phys. B* **259–261**, 1157–1158 (1999).
53. Purans, J., Kuzmin, A., Parent, P. & Laffon, C. X-ray absorption study of the electronic structure of tungsten and molybdenum oxides on the O K-edge. *Electrochim. Acta* **46**, 1973–1976 (2001).
54. de Groot, F. M. F. et al. Oxygen 1s x-ray-absorption edges of transition-metal oxides. *Phys. Rev. B* **40**, 5715–5723 (1989).
55. Zimmermann, R. et al. Electronic structure of 3d-transition-metal oxides: on-site Coulomb repulsion versus covalency. *J. Phys.: Condens. Matter* **11**, 1657–1682 (1999).
56. Aubrey, M. L. et al. Electron delocalization and charge mobility as a function of reduction in a metal–organic framework. *Nat. Mater.* **17**, 625–632 (2018).

57. Cazzanelli, E., Vinegoni, C., Mariotto, G., Kuzmin, A. & Purans, J. Raman study of the phase transitions sequence in pure WO$_3$ at high temperature and in H$_x$WO$_3$ with variable hydrogen content. *Solid State Ion.* **123**, 67–74 (1999).

58. Li, G., Zhou, S., Wang, P. & Zhao, J. Halogen-doping in LiCoO$_2$ cathode materials for Li-ion batteries: insights from ab initio calculations. *RSC Adv.* **5**, 107326–107332 (2015).

59. Lubomirsky, I. Stress adaptation in ceramic thin films. *Phys. Chem. Chem. Phys.* **9**, 3701–3710 (2007).

60. Wang, W., Janotti, A. & Walle, C. G. Vd Phase transformations upon doping in WO$_3$. *J. Chem. Phys.* **146**, 214504 (2017).

61. Sawa, A. Resistive switching in transition metal oxides. *Mater. Today* **11**, 28–36 (2008).

62. Shibuya, K. & Sawa, A. Modulation of Metal–Insulator Transition in VO$_2$ by Electrolyte Gating-Induced Protonation. *Adv. Electron. Mater.* **2**, 1500131 (2016).

63. Valov, I. et al. Nanobatteries in redox-based resistive switches require extension of memristor theory. *Nat. Commun.* **4**, 1771 (2013).

64. Grey, P. et al. Solid state electrochemical WO$_3$ transistors with high current modulation. *Adv. Electron. Mater.* **2**, 1500414 (2016).

65. Kresse, G. & Joubert, D. From ultrasoft pseudopotentials to the projector augmented-wave method. *Phys. Rev. B* **59**, 1758–1775 (1999).

66. Kresse, G. & Furthmüller, J. Efficient iterative schemes for ab initio total-energy calculations using a plane-wave basis set. *Phys. Rev. B* **54**, 11169–11186 (1996).

67. Schimka, L., Harl, J. & Kresse, G. Improved hybrid functional for solids: the HSEsol functional. *J. Chem. Phys.* **134**, 024116 (2011).

Author contributions

B.Y., J.L. and J.D.A. designed, initiated and supervised the project. X.Y. designed, fabricated, and tested the device, with help from W.L., M.O., S.R., and N.E. Material characterization was performed by X.Y., with help from D.K. on the XPS. I.W. and A.H. contributed to the XAS measurement and data interpretation. K.K. conducted the first-principles calculations. All authors discussed the results. X.Y., B.Y., J.L., and J.D.A. wrote the paper.

Competing interests

The authors declare no competing interests.

Additional information

Supplementary information is available for this paper at https://doi.org/10.1038/s41467-020-16866-6.

Correspondence and requests for materials should be addressed to J.A.d.A., J.L. or B.Y.

Peer review information *Nature Communications* thanks the anonymous reviewers for their contribution to the peer review of this work. Peer reviewer reports are available.

Reprints and permission information is available at http://www.nature.com/reprints

Publisher's note Springer Nature remains neutral with regard to jurisdictional claims in published maps and institutional affiliations.

Supplementary information:

Protonic Solid-State Electrochemical Synapse for Physical Neural Networks

Xiahui Yao[1], Konstantin Klyukin[2], Wenjie Lu[3], Murat Onen[3], Seungchan Ryu[4], Dongha Kim[2], Nicolas Emond[2], Iradwikanari Waluyo[5], Adrian Hunt[5], Jesús A. del Alamo[3,*], Ju Li[1,2,*] and Bilge Yildiz[1,2,*]

1. Department of Nuclear Science and Engineering, Massachusetts Institute of Technology, 77 Massachusetts Avenue, Cambridge, Massachusetts, 02139, USA

2. Department of Materials Science and Engineering, Massachusetts Institute of Technology, 77 Massachusetts Avenue, Cambridge, Massachusetts, 02139, USA

3. Department of Electrical Engineering and Computer Science, Massachusetts Institute of Technology, 77 Massachusetts Avenue, Cambridge, Massachusetts, 02139, USA

4. Department of Mechanical Engineering, Massachusetts Institute of Technology, 77 Massachusetts Avenue, Cambridge, Massachusetts, 02139, USA
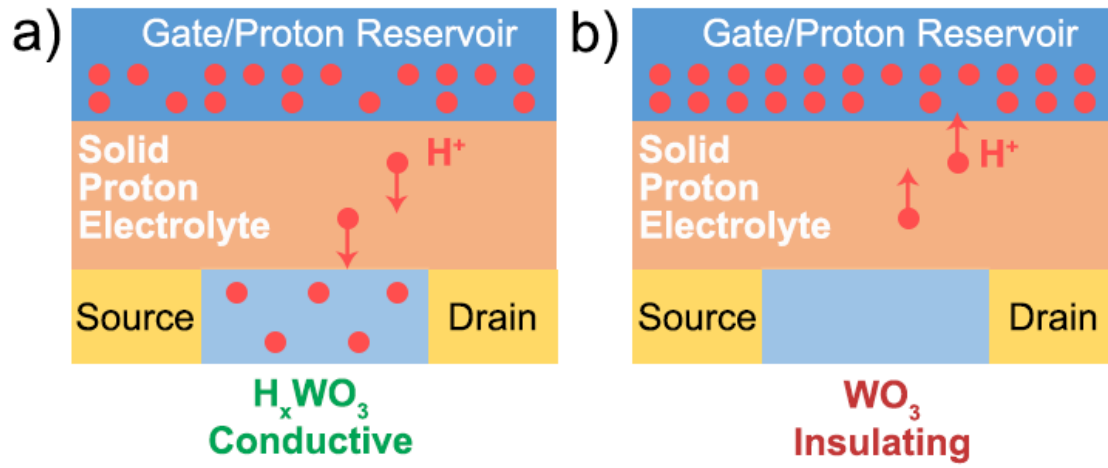
5. National Synchrotron Light Source II, Brookhaven National Laboratory, Upton, New York, 11973, USA

[*] byildiz@mit.edu, liju@mit.edu, alamo@mit.edu

Supplementary figures:

Supplementary Figure 1. a) Positive gating current applied on the gate allows proton intercalating into the channel and increases its conductance. b) Reversed polarity of the gate current de-intercalates the protons from the channel and reduces its conductance.
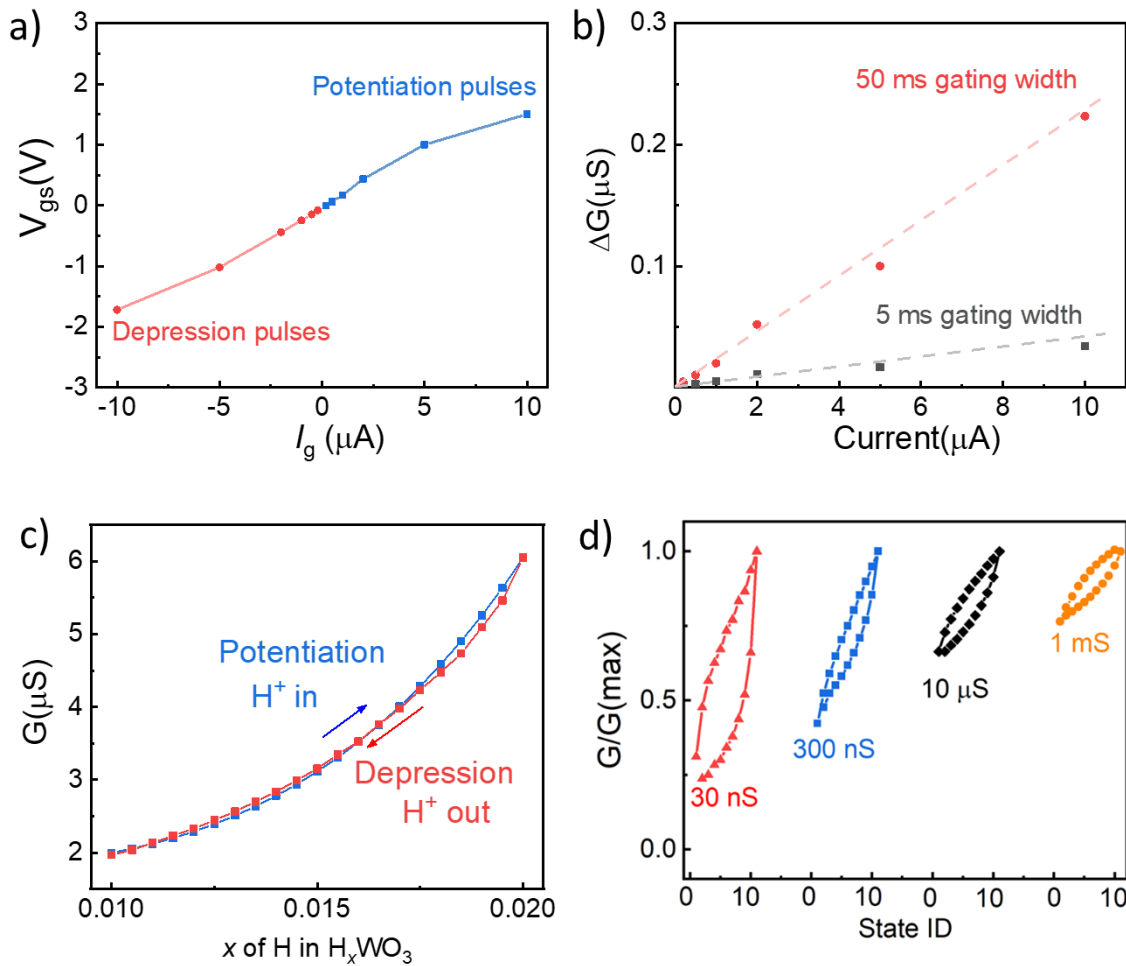
Supplementary Figure 2. a) Dependence of gating voltage on gating current with 5 ms pulsing width. The most energy consuming operation in a hardware neural network is the programing of the weights.[1] This is especially true when the programming process involves the movement of large cations or anions as in the conductive filament mechanism, or Joule heating in the phase change mechanism.[2] Our device is characterized by a small gating voltage.

b) Dependence of channel conductance change on different gating current with 5 ms or 50 ms constant current pulse width. In this electrochemical synapse, the conductance change of the active material depends on the amount of injected charge (Q).[3] This is determined by the integration of gate current over time. Constant-voltage bias typically generates a non-linear current response, which depends on the kinetics of the ion motion and the relative difference between the biasing voltage and the equilibrium chemical potential. On the other hand, the constant-current mode provides a linear relationship between Q and t, eliminating the need to keep track of the Open

Circuit Potential (OCP) as in the constant gate voltage pulse mode. This linearity enables the rational design of gating protocols to achieve the desired potentiation/depression behavior of the electrochemical synapse.

c) Good symmetrical operation when operated in the lower conductance regime of the demonstrated device. Each data point represents a stable conductive state after a protonating or de-protonating pulse (20 potentiation + 20 depression).

d) Comparison of 10 states at different conductance level. The four color represent different starting conductance level. Red: 30 nS, Blue: 300 nS, Black: 10 μS, Orange: 1 mS. The conductance data of the ten states obtained with the 10 potentiation and 10 depression pulses are normalized to maximum conductance obtained in the process. The plot clearly shows that the same amount of proton result in difference in the G_{max}/G_{min} ratio at different conductance level. The area of the loop represents the hysteresis between the potentiation and depression.
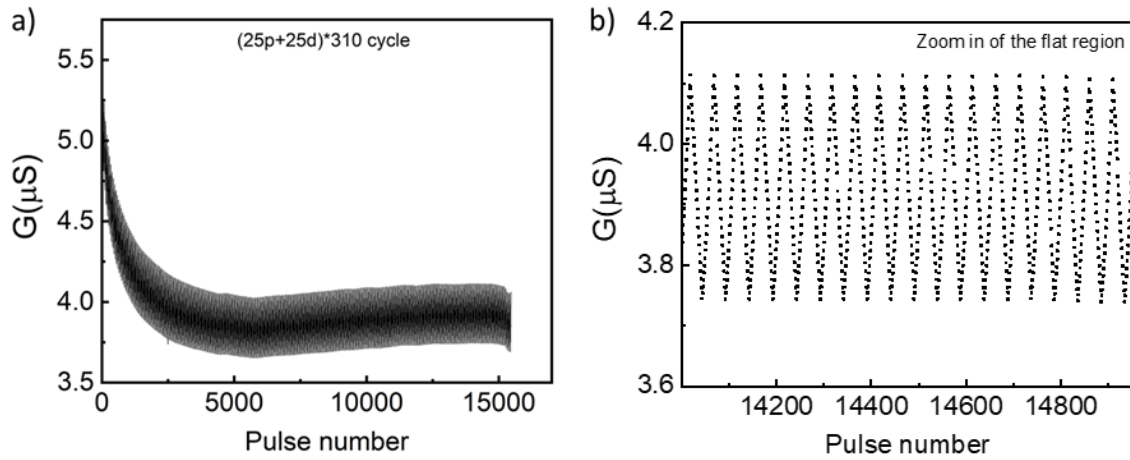
Supplementary Figure 3. a) Cycling behavior in the low conductivity region, with 25 potentiation pulses and 25 depression pulses for each cycle, lasting 310 cycles. The device is un-encapsulated. b) Zoomed in view of the flat region. Each dot represents the average conductance measured over the 1 second period between two pulses.
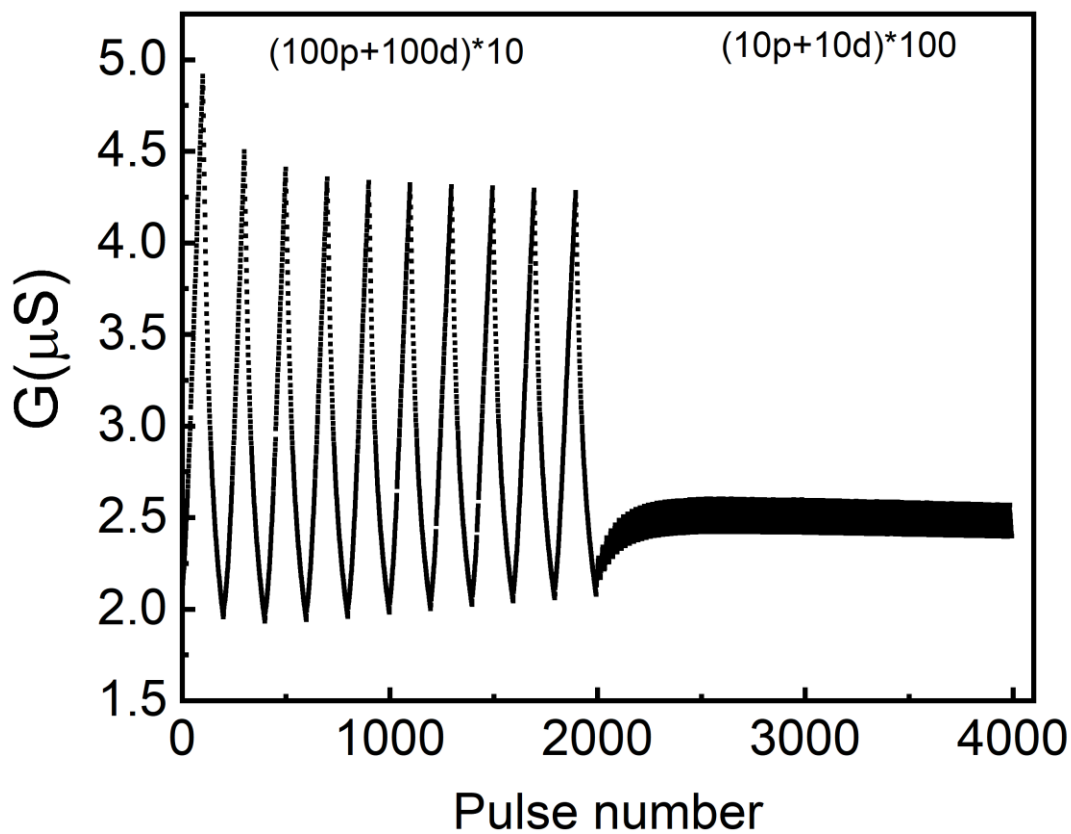
Supplementary Figure 4. Cycling behavior at low conductivity region, with dependence of pulse number per cycle as noted on over the curve. This plot clearly shows the dependence of G_{max}/G_{min} on the pulse number used in the gating. Also, the endurance of the unencapsulated device is demonstrated again here.
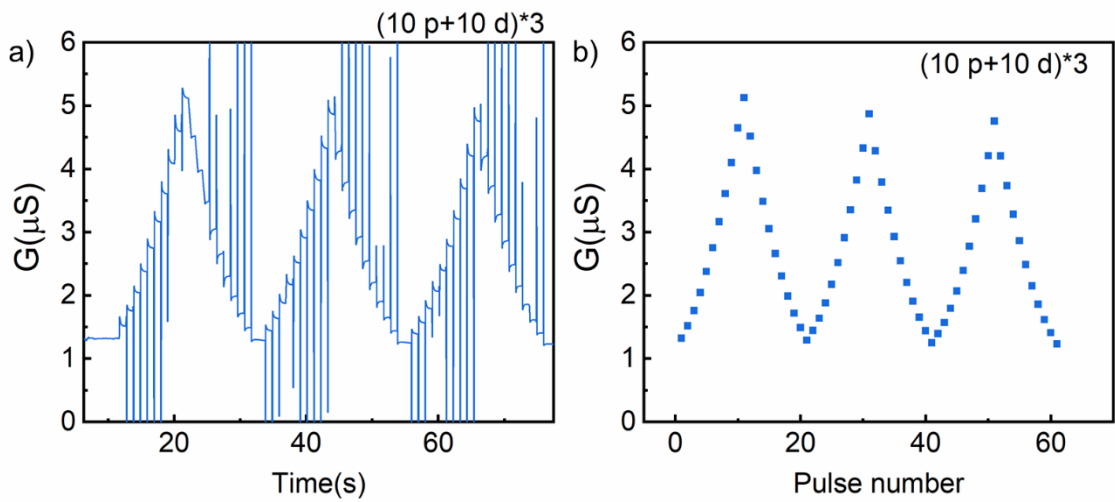
Supplementary Figure 5. Switching behavior of the device with WO_3 annealed at 400 °C for 1h instead of 50°C. a) The raw data of conductance *vs* real operating time, demonstrating the stable state after each pulse. b) Extracted states *vs* the pulse number to demonstrate the reversibility and low hysteresis of the cycling.
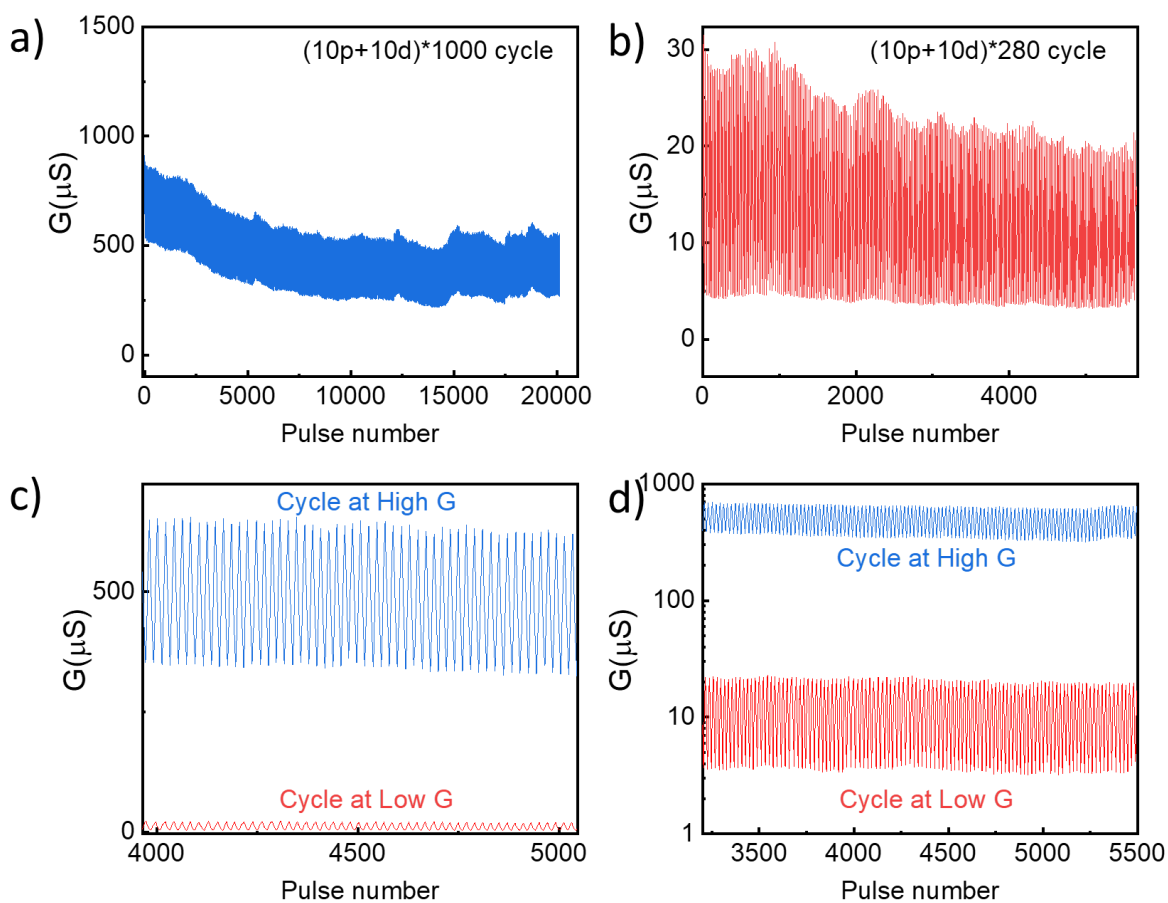
Supplementary Figure 6. Cycling behavior of encapsulated device, with dependence of pulse number per cycle as noted on over the curve. The device is encapsulated by UV-curable polymer and further covered by insulating epoxy after hydrogenation, to isolate the de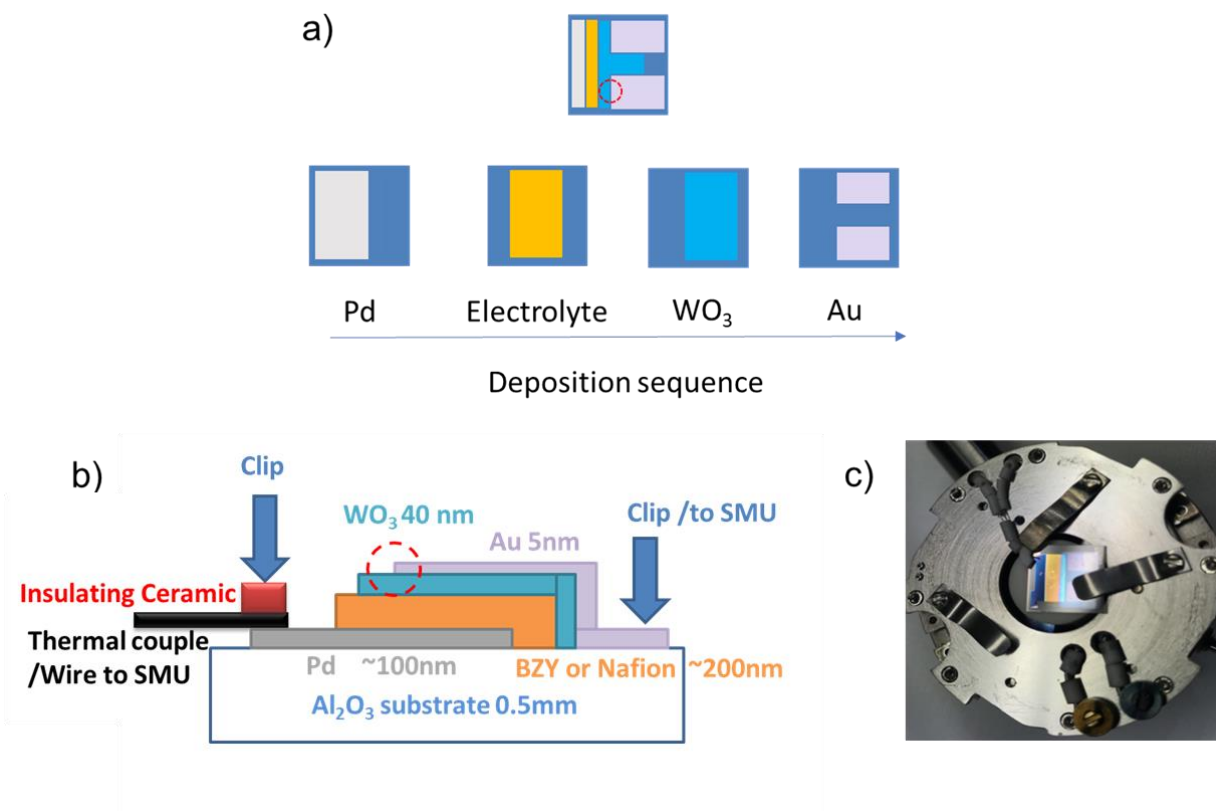vice from ingression of oxygen from ambient air. a) cycling at high conductance regime, b) cycling at low conductance regime, c) zoomed in view comparing the cycling in linear scale conductance. The amplitude of the pulsing current level (0.5 µA) and width (50 ms) are identical for these two regimes. d) Logarithmic scale of conductance of the zoomed in view of cycling data, with clear indication of G_{max}/G_{min} ratio being difference for the same amount of hydrogen insertion/remove in different conductance regimes.

a)

Pd Electrolyte WO$_3$ Au

Deposition sequence

b)

Clip

WO$_3$ 40 nm

Au 5nm

Clip /to SMU

Insulating Ceramic

Thermal couple /Wire to SMU

Pd ~100nm

BZY or Nafion ~200nm

Al$_2$O$_3$ substrate 0.5mm

c)

Supplementary Figure 7. a) The deposition sequence of the inversely ordered device for X-ray absorption and X-ray photoelectron spectroscopy measurements. b) Cross-sectional schematic of the device. The region for probing was noted as the red dashed circle. c) Picture of the test device mounted on the in-situ XAS sample holder with biasing capability before measurement.
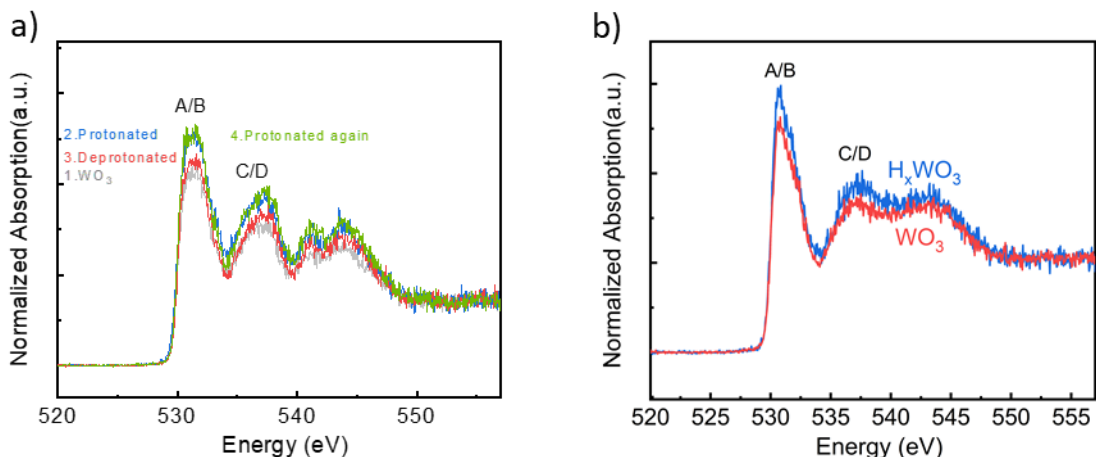
Supplementary Figure 8. O K-edge XAS measured on the WO_3 region with the following operation sequence:

1. WO_3: Measured before effective biasing, with H_2 and H_2O presence in the chamber

2. Protonated: Negative current was applied on the WO_3 (positive I_g on Pd gate electrode, $+10$ μA, ~15min), measurement is made after bias is removed.

3. Deprotonated: Positive current was applied on the H_xWO_3 (negative I_g on Pd gate electrode -40 μA, ~15min), measurement is made after bias is removed

4. Protonated again: Negative current was applied on the WO_3 (H_xWO_3) again, measurement is made after bias is removed

a) The solid electrolyte used in this sample was $BaZr_{0.8}Y_{0.2}O_3$, a well-known ceramic proton conductor. The biasing was operated at 340°C to compensate the low proton conductivity as a result of the low water and hydrogen vapor pressure allowed for *in operando* XAS system, in which $p(H_2) = 400$ mTorr, $p(H_2O)=5$ mTorr.

b) The sample with Nafion as electrolyte also exhibits the similar peak intensity change after protonation. Due to the inversed deposition sequence and thermal stability of Nafion, the WO_3 grown on sample b) was used in the as deposited form without the annealing step at 450 °C (amorphous WO_3).
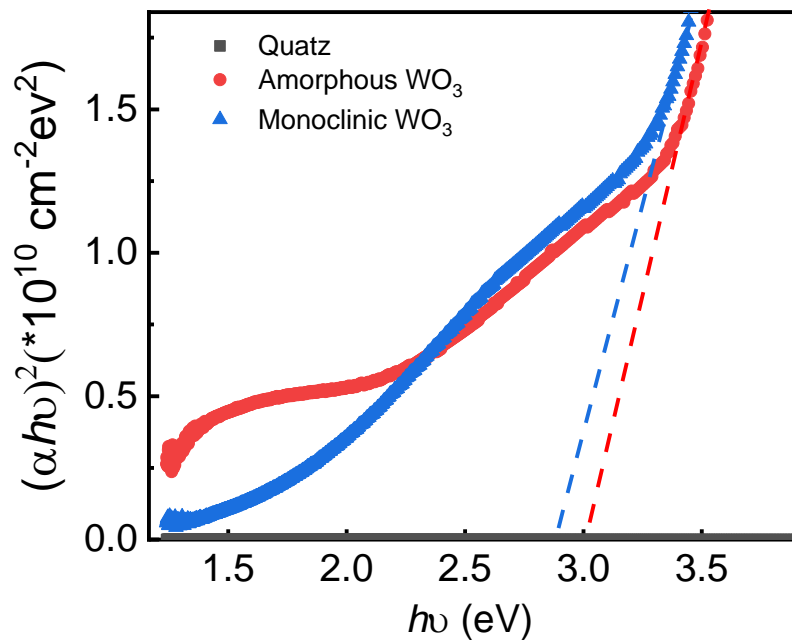
Supplementary Figure 9. Light absorption bandgap of WO_3 was measured to be from 2.8 eV to 3.0 eV with different crystal structure. The amorphous WO_3 was measured directly after deposition form reactive sputtering. The monoclinic WO_3 was obtained by further anneal the as-deposited sample in ambient air for 1 hour at 450 °C.
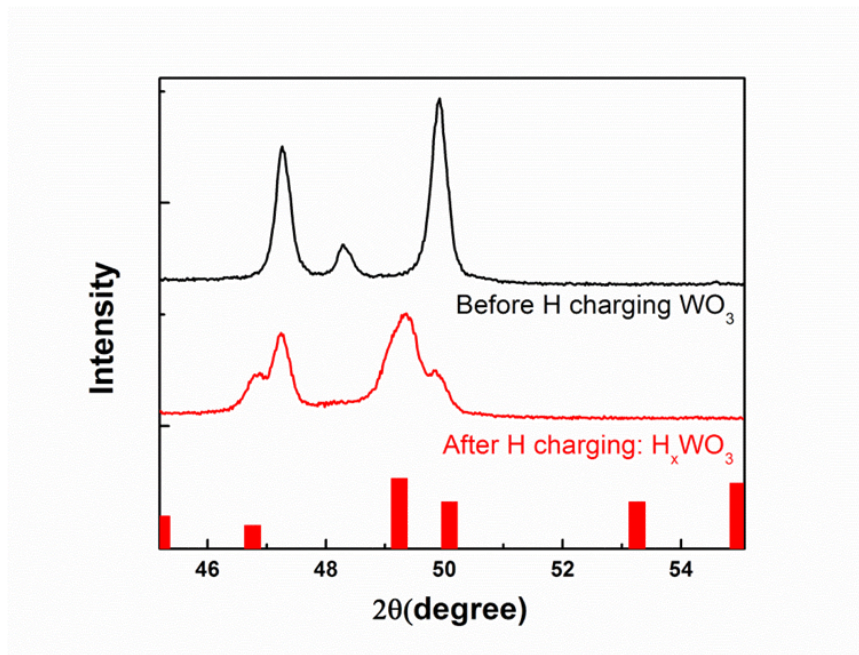
Supplementary Figure 10. High angle region of the XRD pattern comparing WO_3 and protonated H_xWO_3.
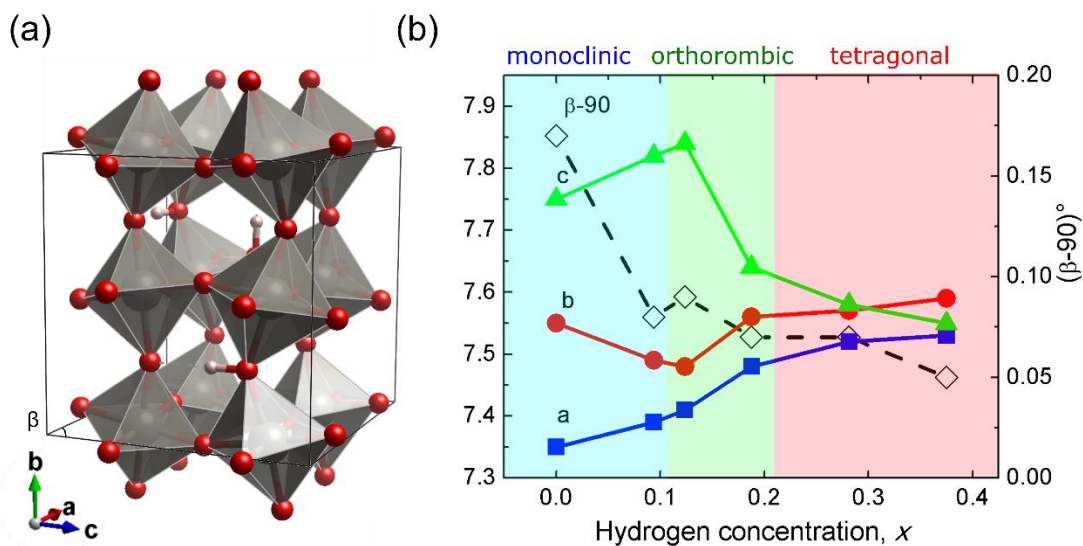
Supplementary Figure 11. Static DFT calculations (T=0 K) are employed to monitor evolution of WO_3 lattice parameters and β-angle upon hydrogen insertion. (a) Monoclinic unit cell of WO_3 was used to model the most energetically favorable configuration before hydrogen uptake (x=0). Tetragonal crystal structure of H_xWO3 was found stable at $x = 0.375$ assuming a homogeneous distribution of H over WO_3 lattice. Intermediate hydrogen concentrations were simulated by varying a partial occupancy of H pseudo atoms as implemented in VASP. (b) Evolution of structural parameters indicates that the interaxial angles approach 90° upon H insertion and transition between monoclinic and tetragonal phases occurs through orthorhombic phase. These results are in good qualitative agreement with our X-ray diffraction data shown in Figure 4 d and previous theoretical simulations on phase transformations caused by charge doping of WO_3.[4]

Computational Details. We used the hybrid functional of Heyd, Scuseria, and Ernzerhof corrected for solids (HSEsol), 4 × 4 × 4 Γ-centered k-point mesh and energy cutoff of 500 eV. All calculations are converged until the residual forces are below 0.04 eV/Å.
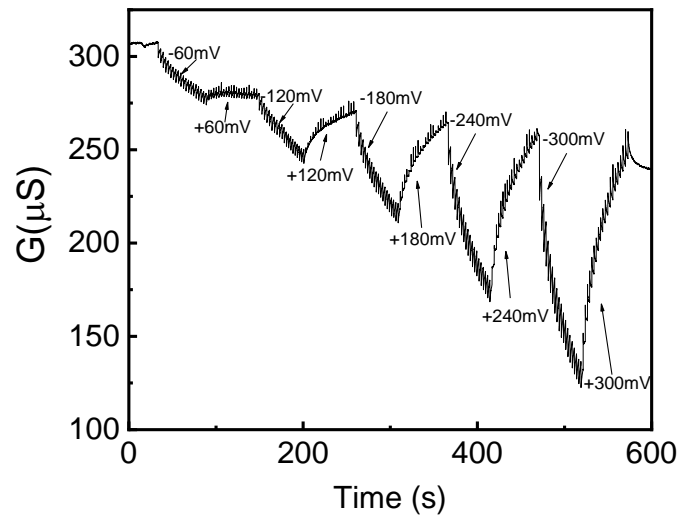
Supplementary Figure 12. Constant voltage gating of the channel WO_3 and corresponding conductance change. Positive or negative of the voltage level indicated on the plot was used to achieve the potentiation/depression behavior. With proper tuning of the voltage selected in the constant voltage gating, symmetrical switching can also be obtained. But it requires exploration of parameters specific to each device, or the same device at different state of charge (H content). In contrast, constant current pulsing neglects such variation, and only induces the fixed amount of protons with the same pulsing width. Therefore, although similar switching behavior can be achieved by constant voltage gating, constant current gating is still considered advantageous.
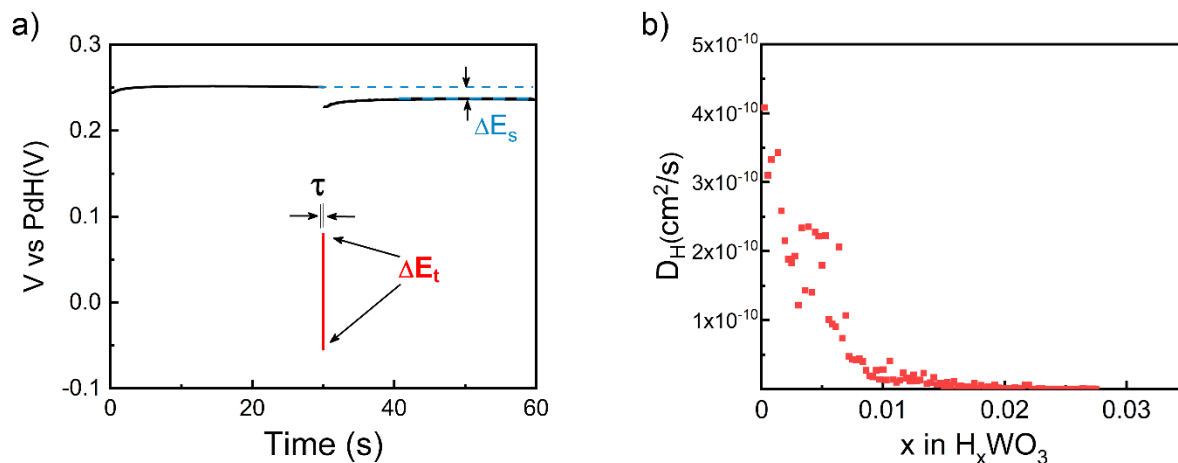
Supplementary Figure 13. a) Example data for one pulse (red trace) and the open circuit potential evolution (black trace) before and after the pulse in the Galvanostatic Intermittent Titration Technique (GITT) experiment. τ stands for the duration of each constant current pulse, ΔE_s is the steady-state chemical potential change as the result of the current pulsing, and ΔE_t reflects the voltage change during the constant current pulse. The voltage notation here is the channel (WO_3) vs the gate (PdH_x), reverse the value of the V_{gs}. b) The diffusivity of proton inside H_xWO_3 obtained from the GITT experiment in the low hydrogen content regime where x is between 0 to 0.03.
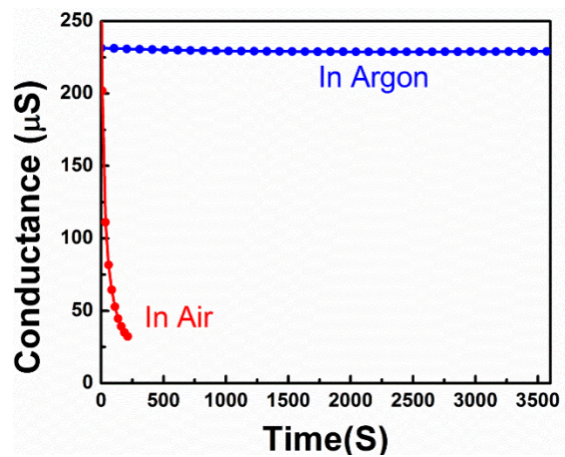
Supplementary Figure 14. Stability comparison of high conductance state of H_xWO_3 in air and in argon atmosphere. A quick degradation is observed when the unencapsulated device is exposed to air. A stable retention of the conductance is observed when the device is protected under argon inert atmosphere.
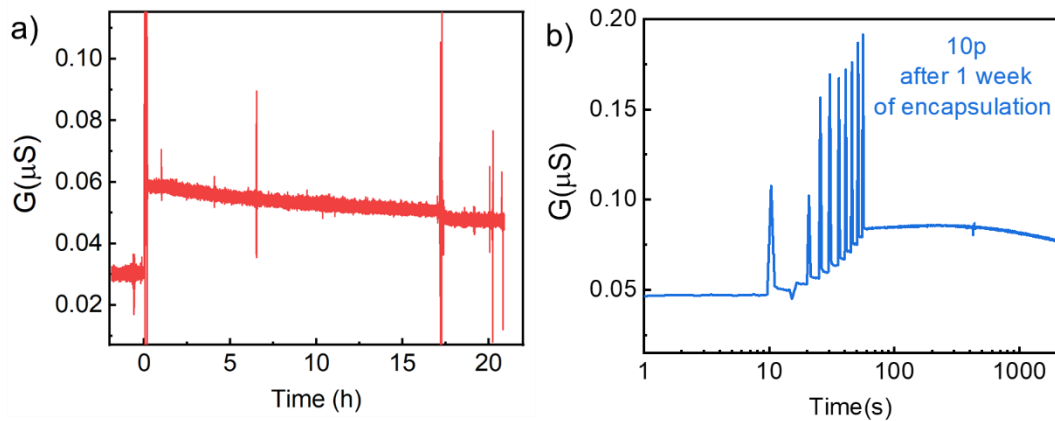
Supplementary Figure 15. Retention of a) an encapsulated device fresh after preparation with linear time scale and b) the encapsulated device after 1 week of preparation with log time scale. The increase of conductance was induced by a potentiating pulse train containing 10 constant current pulses with 200 nA amplitude and 50 ms width. The pulse train started at the time mark of 10 s. Between two pulses, the gating circuit was set as open circuit for 5 s, so that the channel conductance can be measured. After the pulse train, the gating circuits was opened again for long term retention measurement. The conductance of the channel is stable for tens of hours (a) and hundreds of seconds before degradation (b) demonstrating the robustness of the encapsulated device. Currently for our proof-of-concept device, the encapsulation approach is not ideal, and rather rudimentary. So any data that we collect with this approach will not represent the true potential of this device for endurance and retention. Characterization of the endurance and retention in properly encapsulated devices warrants future work.
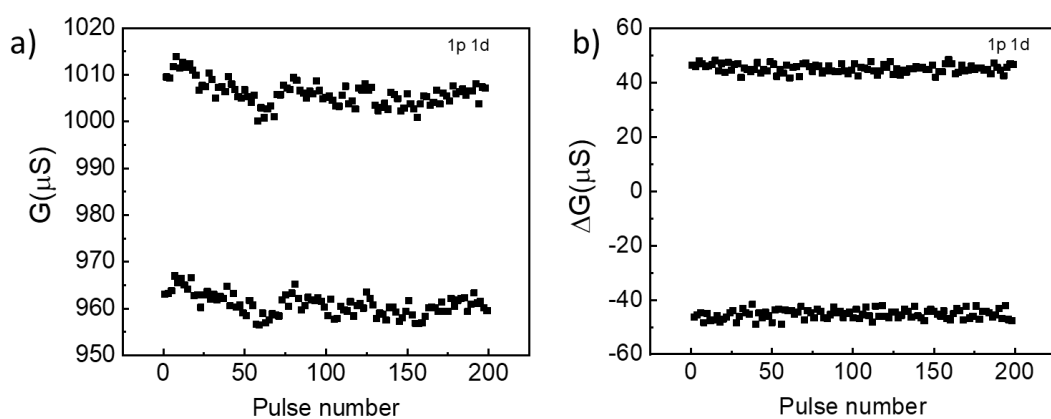
Supplementary Figure 16. a) Conductance (G) and b) conductance change (ΔG) with alternating 1 potentiation and 1 depression operation for 100 cycles. Reproducible switching behavior with low hysteresis is evident.

The switching behavior is more reversible with less proton exchanged for each cycle. We have demonstrated the good symmetry with reduced current density for each pulse in Figure 1d and the dependence of pulse number in each cycle in Figure 2b-d. This figure here provides additional information on pulse number dependence, where only 1 potentiation and 1 depression operation are used to induce the resistive behavior. Highly reproducible state change is evident here for 100 cycles. Each pulse has ±500 nA amplitude and 5 ms width.

Supplementary Table 1. Calculation of hydrogen content in WO_3 film during in-situ XRD

Sample label	Current (mA)	Time (s)	H (mol)	WO_3 (mol)	x in H_xWO_3
10 min	0.001	600	6.22×10^{-9}	1.28×10^{-7}	0.049
23 min	0.001	1380	1.43×10^{-8}	1.28×10^{-7}	0.112
54 min	0.001	3240	3.36×10^{-8}	1.28×10^{-7}	0.263

The dimension of WO_3 film: 0.826 cm $\times$ 0.5 cm $\times$ 100 nm.

Device configuration from bottom to top: Au/WO_3/Nafion/Pd.

Gate current bias: 1 uA.

Supplementary discussion 1: Gating strategy of electrochemical synapses

Gating by voltage signal is widely adopted in the literature to induce resistive switching due to its simplicity of implementation.[5] Typical reported gating voltage values range from several volts to tens of volts. Very often, the gating voltage used as a descriptor to indicate the final state of the sample.[6,7] Here we want to emphasize that, in such electrochemical three-terminal synapse devices, there can be a difference between the applied voltage and the equilibrium chemical potential. Since the gating process is essentially the charging of a capacitor, a good analogy is that the voltage to charge the capacitor (V_g here) and the voltage that the capacitor will retain (Open Circuit Potential, or chemical potential here) will be different before the capacitor is fully charged (sufficiently long charging time is allowed). And such difference could be one major reason for the lack of consistency of the gating voltages in the literature.[6,8-10] There are two major aspects to consider.

First, the voltage applied during the ionic gating is a dynamic voltage, not a steady-state chemical potential. Different from traditional electronic devices, in which only electrons or holes are mobile, the gating signal in the ionic device has to be converted into the flow of ions at the electrode-electrolyte interface. Therefore, the applied voltage contains three components: the chemical potential difference between the two electrodes, ionic ohmic loss across the electrolyte, and the Nernst overpotential at the electrode to drive the electron-ion exchange at the interface. For ionic gating, only the material status change, reflected by the chemical potential, is important to determine the channel conductivity. But to achieve the same amount of chemical potential change, the total applied voltage needed will be different across different material systems. This results in the scatter of gating voltage values that is observed in the literature. In addition, the absence of a clear indication of the reference for the applied voltage (the potential of electrochemical reaction at the counter electrode) is another major source of this inconsistency. Moreover, even for the same material system, the contribution from these three terms could be different at different conduction states of the material. All these factors result in the unpredictability of the gating voltage needed for switching, even for the same type of device. As an example, we adopted the constant voltage gating mode to induce the conductance change in Supplementary Figure 12. Although proper switching behavior can be induced, one cannot rationally design what the gating voltage should be, to achieve symmetrical switching behavior without trial and error for each different device.

Second, even if the biasing voltage-chemical potential correlation can be properly established, the time needed to reach the equilibrium between chemical potential on the surface and in the bulk is non-negligible. The mobile ions move from the electrolyte layer into the surface of the active material under the driving force of an electric field, and diffuse further into the bulk material to give rise to the change in the property of interest. The diffusivity of ions is typically much lower than electrons, in the order of $10^{-10} \sim 10^{-15}$ cm^2/s. Therefore, the surface to bulk diffusion in the active material process is non-negligible and the time needed to reach equilibrium depends heavily on the diffusion coefficient and the sample thickness. This sluggish diffusion results in a difference between the applied biasing voltage and the final equilibrated chemical potential of the material if only short pulses are applied. Evidence can be found in Supplementary Figure 13a, in which -0.05 V voltage (vs PdH$_x$, this means V$_{gs}$= +0.05 V) is used to potentiate the channel for 5 ms, but the open circuit potential of the channel is only changing from 0.25 V to 0.23 V, this equilibrium potential of 0.23 V is significantly different from the applied bias of -0.05 V. This indicates that the biasing voltage is not a good parameter to describe what final status the device is modulated to. To achieve the device status defined by pulsing voltage, much longer biasing time than what has been reported in the literature (ms level) or smaller voltage difference compared with open circuit voltage will be necessary. This can be estimated from the diffusion time equation below, in which t stands for the time needed for diffusion to the length of x with the diffusion coefficient of D.

$$t \approx \frac{x^2}{2D}$$

Based on these analyses, we propose two directions to minimize the discrepancy. First, we should use constant current gating to obtain deterministic switching behavior. A direct descriptor for the channel status (conductivity) is the proton content in the channel. Regardless of the resulting gate voltage, the constant current gating always delivers a well-defined amount of charge into the active material. Since the correlation between proton concentration and material conductivity has been established (e.g. Figure 2a for WO$_3$), we can quantitatively change the status of the material conductance over a wide range simply by controlling the integral of the current with biasing time. This method is invariant to the detailed condition of the electrolyte, or the gate electrode chemical potential, as long as the gating voltage is within the electrochemical stability window of the electrolyte so the Coulombic efficiency is 100 % and there is not electrical break down.

Second, we should introduce cations with high diffusivity, such as protons, and reduce the dimension of the device. In our demonstration, the proton is intentionally selected as the charge carrier to provide fast diffusion kinetics. To provide evidence of this, we employed Galvanostatic Intermittent Titration Technique (GITT) to probe the diffusivity of proton in our device. This technique utilizes the time dependent relaxation of the open circuit voltage of the device upon the application of electrical gate pulses to quantify the diffusion coefficient of protons in WO_3. We analyze the data by the following simplified equation below[11]:

$$D = \frac{4}{\pi\tau}\left(\frac{n_m V_m}{S}\right)^2\left(\frac{\Delta E_s}{\Delta E_t}\right)^2$$

Here, τ stands for the duration of each constant current pulse, n_m is the quantity of material in moles, V_m is the molar volume of WO_3 (cm^3/mol), S represents contact area between WO_3 and the electrolyte, ΔE_s is the steady-state chemical potential change as a result of the current pulsing, and ΔE_t reflects the voltage change during the constant current pulse (Supplementary Figure 13a)

As demonstrated in Supplementary Figure 13b, the diffusion coefficient of H in H_xWO_3 is of the order of 10^{-10} cm^2/s at the initial protonation stage. This value correlates well with previous literature reports of proton diffusivity in WO_3 measured through liquid protonation.[12] An interesting observation is the reduction of D_H as the degree of protonation increases. This behavior is typically explained by the mechanism of stuffed diffusion channels, originating from protons percolating the fast diffusion channel inside the WO_3 lattice or saturating the grain boundary channel.[13] This implies the states at higher proton content need longer time to reach equilibrium, which can be reflected by the different operating symmetry shown in Figure 2. This observation further highlights the importance of proper selection of operating regime to achieve desired switching properties.

Supplementary discussion 2: Degradation mechanism and mitigation

In the unprotonated state, the low conductance state of WO_3 is very stable.[14] Basically, it is a thermodynamically and kinetically stable material without any known degradation mechanism at room temperature. On the contrary, if left as an open system in the presence of oxygen, the higher conductance states, H_xWO_3, are potentially unstable. H_xWO_3 can lose its conductive state through the following chemical reaction:

$$H_xWO_3 + O_2 = H_2O + WO_3$$
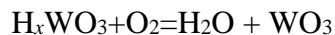
In fact, we do observe quick conductance degradation, within tens of seconds, if our unencapsulated device is exposed to ambient air (Supplementary Figure 14). However, H_xWO_3 itself is thermodynamically stable. This means that if not exposed to oxygen, the degradation of the material should be eliminated. Indeed, the devices kept under inert atmosphere showed long-term retention of the conductance (Supplementary Figure 14).

To demonstrate the long-term stability in a more realistic condition, we employed a polymer encapsulation approach to package our device. The encapsulated device can be tested in ambient air without the protective atmosphere. The cycling performance has been shown in Supplementary Figure 6 before and the retention of the state is shown below in Supplementary Figure 15. The device is still operable after weeks of encapsulation before optimization of the packaging approach, demonstrating the robustness of the device. We envision, with better sealing, better retention can be obtained.

Another potential degradation mechanism is the loss of protons as hydrogen gas or through diffusion into the substrate during the electrochemical cycling between the PdH_x and WO_3. As an electrochemical process, the Faradaic efficiency is desired to be 100% but the realistic efficiency is often less than ideal. We do not have any evidence of this issue in our experiments. However, such a challenge could show a cumulative effect over very large number of cycles.

Our strategy to mitigate this possible mode of degradation is through the redundant storage of hydrogen in the solid reservoir layer. Two factors are important for this: 1) The solid hydrogen reservoir layer should have a high hydrogen storage capability, and 2) A small concentration of protons should lead to a signification change of the conductance of the channel material. Regarding the first point, palladium is one of the best hydrogen storage materials since it can hold up to 1

hydrogen atom per unit Pd. Properly tuning the relative thickness ratio between the Pd and the WO_3 active layer can provide the desired hydrogen utilization fraction over the targeted life cycle of the device.

However, the thickness of hydrogen storage material involved should still be small. That brings forth the second point, a small amount of hydrogen should give rise to large enough modulations of conductivity. In order to serve as accurate accelerators in AI, the conductance range of the device should be at least one order of magnitude[15]. This device needs only as low as 1 mole percent of H to achieve one order of magnitude on/off ratio, as shown in low H content region in Figure 2a. Therefore, even if the Faradaic efficiency is less than 100%, we expect that the endurance of the device can still be satisfied.

Supplementary discussion 3: Dependence of Open Circuit Potential on the hydrogen content

Simultaneous transitions in the slope of the OCP between the channel (H_xWO_3) and gate (PdH_x) and the channel conductivity are seen in Figure 2a. This gives further evidence that the cause of transitions in the conductivity is likely related to a phase change in the channel material. As described in the Methods, we are operating this device (without an encapsulation) in a hydrogenated atmosphere for the evaluation of the intrinsic property of the active material. In this condition, the PdH_x gate electrode serves as a reliable reference electrode at open-circuit condition because it produces a stable chemical potential in contact with the Nafion when there is no net current. Therefore, the OCP measured here reflects the chemical potential of H_xWO_3 with respect to PdH_x. The change of the dependence of the chemical potential on x in H_xWO_3 indicates that different phases of H_xWO_3 are involved in the different regimes. Structural characterization presented in Figure 4d further support such phase transition.

Supplementary discussion 4: O:W stoichiometry

We used the W4f region to estimate the non-stoichiometry. The W $4f_{7/2}$ peak was deconvoluted into two peaks. The main peak was assigned to be W^{6+} and a very small shoulder peak was assigned to the reduced W due to oxygen vacancy. The relative percentage of these two peaks are 95.5% vs 4.5%. Based on the peak position, this reduced W has the oxidation state between W^{6+} and W^{5+}, if we assume them to be 5+ for the ease of calculation, we get the O:W ratio as 2.977. To be noted, this number is underestimated because the assumption we made, so we expect the true value to be higher than this and closer to 3.

Supplementary References

1. Deng, L. *et al.* Energy consumption analysis for various memristive networks under different learning strategies. *Phys. Lett. A* **380,** 903-909 (2016).
2. Yang, J. J. S., Strukov, D. B. & Stewart, D. R. Memristive devices for computing. *Nat. Nanotech.* **8,** 13-24 (2013).
3. Chua, L. Resistance switching memories are memristors. *Applied Physics A* **102,** 765-783 (2011).
4. Wang, W., Janotti, A. & Walle, C. G. V. d. Phase transformations upon doping in WO_3. *J. Chem. Phys.* **146,** 214504 (2017).
5. Sawa, A. Resistive switching in transition metal oxides. *Materials Today* **11,** 28-36 (2008).
6. Katase, T., Onozato, T., Hirono, M., Mizuno, T. & Ohta, H. A transparent electrochromic metal-insulator switching device with three-terminal transistor geometry. *Sci. Rep.* **6,** 25819 (2016).
7. Shibuya, K. & Sawa, A. Modulation of Metal–Insulator Transition in VO_2 by Electrolyte Gating-Induced Protonation. *Adv. Electron. Mater.* **2,** 1500131 (2016).
8. Grey, P. *et al.* Solid State Electrochemical WO_3 Transistors with High Current Modulation. *Adv. Electron. Mater.* **2,** 1500414 (2016).
9. Leng, X. *et al.* Insulator to metal transition in WO_3 induced by electrolyte gating. *npj Quantum Mater.* **2,** 35 (2017).
10. Yang, J.-T. *et al.* Artificial Synapses Emulated by an Electrolyte-Gated Tungsten-Oxide Transistor. *Adv. Mater.* **30,** 1801548 (2018).
11. Zhu, Y. & Wang, C. Galvanostatic Intermittent Titration Technique for Phase-Transformation Electrodes. *J. Phys. Chem. C* **114,** 2830-2841 (2010).
12. Randin, J. P. & Viennet, R. Proton Diffusion in Tungsten Trioxide Thin Films. *J. Electrochem. Soc.* **129,** 2349-2354 (1982).
13. Vértes, Á. & Schiller, R. Concentration-dependent diffusivity: Hydrogen percolation in WO_3. *J. Appl. Phys.* **54,** 199-203 (1983).
14. Ramana, C. V., Utsunomiya, S., Ewing, R. C., Julien, C. M. & Becker, U. Structural Stability and Phase Transitions in WO_3 Thin Films. *J. Phys. Chem. B* **110,** 10430-10435 (2006).
15. Gokmen, T. & Vlasov, Y. Acceleration of Deep Neural Network Training with Resistive Cross-Point Devices: Design Considerations. *Front. Neurosci.* **10,** 333 (2016).

Reviewers' comments:

Reviewer #1 (Remarks to the Author):

Emond et al: This interesting paper deals with a WO3-based device, the conductivity of which can be modified by electrochemically pumping hydrogen in and out. I.e., the conductivity of the channel can persistently be changed back and forth, not only on/off but with multiple steps in between. Such devices termed "electrochemical synapses" could be very beneficial for analog implementations of neuronal networks. The principle has been realized before with other materials (organic semiconductors, or WO3 with lithium insertion) but the present combination of WO3 with hydrogen pumping is expected to be advantageous with respect to long-term stability and energy consumption.
The physical mechanism of changing WO3 conductivity by hydrogen insertion=reduction is straightforward (and well supported by XPS and DFT results), also the appearance of the different regimes in fig. 2a.
It is important to explore several options how to realize such devices (which channel material, modified by which ion insertion, which operation mode...), and thus overall I recommend publication.

Some points related to the practical applicability should be discussed in more detail:
* regarding the multi-state capability, authors should be more specific which magnitude of conductance change is regarded necessary for reliable and reproducible access of one state, and how many states can realistically be implemented in one cell
* low hysteresis is decisive for multi-state operation. I'm a bit surprised that even under current control quite big hysteresis occurs under some conditions, e.g. fig. 2c,d. Any idea why, and how to improve that?
* According to the reported results, current gating is preferred as operation mode over voltage gating. Please comment if this would lead to any significant complications for construction of real devices comprising many such synapse cells (current is more difficult to control than voltage), or how big the chance is to get good performance also in voltage gating
* it would be good to comment on the scatter in conductance between a larger number of nominally identical cells (i.e. how reliably can the number of cells be scaled up)
* the cells need humidity in the Nafion layer, and oxygen in- and/or hydrogen out-diffusion must be avoided. Authors report some preliminary encapsulation tests, but longer times than in fig S14 should be reported
* a related issue: Nafion is an acidic polymer. Any long-term degradation in contact with palladium hydride (the hydrogen reservoir) by releasing hydrogen from proton+hydride ions, and incorporation of Pd2+ into Nafion for charge compensation?

Reviewer #2 (Remarks to the Author):

In this manuscript the authors present a very complete work on the development of three-terminal synapses based on proton intercalation in inorganic materials. The work is very complete, as it provides clear information about the fabrication of the devices, complete morphological and electrical characterization, and atomistic modelling. The electrical characteristics measured are impressive, specially the linearity achieved and the controllability of the potentiation and depression processes. The conductance modulation mechanism is clearly identified using "in operando" chemical measurements. Overall, the work provides important insights in its field of research, and the reliability of the findings is higher than in most reports in this field due to the multiple and high quality techniques used. In my opinion, this work is above the level of most others in the field, and for that reason I would like to recommend its publications in Nature Communications.

The only weakness that I see, which the authors should definitely further discuss, is the integration capability of this work:

1- First of all, they use devices with channels of 100 um (is that the length or the width?). These devices are very big. Did the authors try to do smaller devices? This is highly recommended in order to observe if the findings also apply to miniaturized devices.

2- Moreover, as the authors wrote the word "computing" in the title of their abstract and because the introduction of their paper is discussing about "in memory computing", the authors should discuss what is the potential of their device for computation, which in its current form seems to be unclear to me. The authors should clarify which kind of computation may be done with their device and the path towards such implementation. I do not think it is necessary they demonstrate such computation, but they may reference some works that did such things.

3 – The authors should also indicate which is the advantage and disadvantage of their devices compared to two-terminal resistive switching devices. I think two-terminal resistive switching devices are the most commonly used in most companies, and therefore it seems to me that they have most potential to end up being the hardware for such "in memory computing". Therefore, from a technological point of view, the authors should clarify the potential of their work.

The work is really good, I really enjoyed reading it, but the authors should provide more practical information about the technological potential of their work. I also recommend to remove the word "computing" from the title; some readers may get too excited when seeing the title and later disappointed when reading the manuscript, as there is not computing in this manuscript. In the future, the authors may try to associate different devices to solve a complex problem. They may even indicate such thing in the conclusions to encourage the community to work in such application.

Reviewer #3 (Remarks to the Author):

Authors in this work demonstrate a three terminal device based on proton migration. The device shows a great reversibility for analog signal processing under current pulses. They have also performed impressive and careful materials studies both experimentally and theoretically to conclusively reveal the switching mechanism. It is a very interesting and timely work. I strongly recommend it for publication.
I do have some minor comments for the authors to consider.
1. The authors obtained good XAS and XPS results to make comparisons between WO3 and HxWO3, but the exact ratio of O to W of the as-deposited film was not revealed. It would be great if the stoichiometric ratio of O to W is also given in the manuscript. Did author fabricate the WOx film with a non-stoichiometric ratio? How would that affect the performance of the device? How to eliminate the effect of oxygen vacancies migration in WOx channel?
2. The WO3 film was annealed in air at 450 ℃ for 1 h. Please comment on the concentration and effects of nitrogen in the annealed film. In addition, 450C is higher than 400C, which means this process is not 100% fab compatible yet. Would 400C annealing for a longer time achieve the same effect?
3. Please comment on how to control concentration of hydrogen in Pd, nafion and WO3 during fabrication process? How do we know that H has been incorporated into the Pd films? Can phase/structure of PdHx or Hydrogen forward scattering (HFS) help?
4. The relative humidity was 100% during the testing. Does it mean that the devices still somehow rely on water electrolysis? Would any change of the environment humidity affect the proton conductivity of the device? Would the device work well when the test chamber contains hydrogen only? What is the chamber pressure when the devices were tested?
5. In Figure 2b-d, the conductance updating property of the device at low conductance regime

shows a better symmetry than that at middle and high conductance regime. Why does the symmetry of the conductance updating become worse when the concentration of hydrogen increases? Why there is still an asymmetrical updating in low conductance regime? Since the symmetry of conductance updating with 200 pulses looks better than that with 40 pulses and 100 pulses in low conductance regime, would the symmetry be affected by pulse number?

6. In Figure 3b, is there a plausible explanation for that the high resistive state of the device becomes more insulative and low resistive state of the device becomes more conductive after large amounts of cycling?

7. on Page 7, there is a typo, "As demonstrated in Figure 1a, over seven orders …" should be Figure 2a.

8. on Page 9 about Figure 2a "…after 100 positive gating pulses, the conductance of the channel increased from 1 µS to 22 µS, ..." it's a bit confusing here, what is the pulsing sequence, from 100 down counting to 1 in Figure 2b? please use arrows to label them in the figure.

9. The specific pulse height-width that was used to achieve each conductance regime (low, medium and high) should be clearly stated in the caption of Figure 2 or the main text.

10. Endurance to the level of million has not been demonstrated (and not really expected for this paper as well). Is that due to testing time or failure? Please comment on possible failure mode?

11. As the author mentioned, "When the external circuit is cut off (gate is open circuit), the electronic insulating nature of the electrolyte prevents the back flow of electrons, and consequently that of protons too." Therefore, a two-terminal threshold volatile switch was used to provide both selector and threshold functions for programming (e.g. NatMat 16, 396, 2017), without which an array of such devices may only be programmed column-wise or row-wise (not randomly and individually programming a device in the array during learning). Will the device studied here also need such as threshold switch on the gate?

12. A constant current source (compared to a voltage source) is usually not preferred in real circuits due to various reasons.

We thank the reviewers for their constructive comments and support of our work. We have addressed their comments point-by-point in the bullets below, and have made the relevant changes in the manuscript where the changes are highlighted by yellow. We hope our paper is ready for publication in this revised form.

Reviewer #1 (Remarks to the Author):

This interesting paper deals with a WO_3-based device, the conductivity of which can be modified by electrochemically pumping hydrogen in and out. I.e., the conductivity of the channel can persistently be changed back and forth, not only on/off but with multiple steps in between. Such devices termed "electrochemical synapses" could be very beneficial for analog implementations of neuronal networks. The principle has been realized before with other materials (organic semiconductors, or WO_3 with lithium insertion) but the present combination of WO_3 with hydrogen pumping is expected to be advantageous with respect to long-term stability and energy consumption.

The physical mechanism of changing WO_3 conductivity by hydrogen insertion=reduction is straightforward (and well supported by XPS and DFT results), also the appearance of the different regimes in fig. 2a.

It is important to explore several options how to realize such devices (which channel material, modified by which ion insertion, which operation mode...), and thus overall I recommend publication.

Comment: *Some points related to the practical applicability should be discussed in more detail:*

* regarding the multi-state capability, authors should be more specific which magnitude of conductance change is regarded necessary for reliable and reproducible access of one state, and how many states can realistically be implemented in one cell

Response: The number of states achievable, the maximum/minimum conductance ratio (G_{max}/G_{min}), and the relative change of resistance at each pulse depends on the initial hydrogenation state (including zero) and the pulse parameters. In principle, within the same G_{max}/G_{min}, the number of states can be controlled by the amount of charge injection during each pulse. (G_{max}/G_{min} = Number of states × Difference between each state, ΔG, in the linear regime). In the literature, the desired specifications for reliable training of neural networks were outlined by Gokmen and Vlassov, *Front. Neurosci.* **10,** 333 (2016). The specs proposed included a change of resistance at each step to be at least ΔR=100 KΩ, and the min value of the low resistance state to be R=14MΩ, and a minimum of 8-fold tuning of resistance up to 112MΩ. This corresponds to $\Delta G/G$ to be at least 0.7~0.09% $\Delta G/G$ and implies nearly 1000 states should be needed.

Based on our current device characteristics, when the pulsing current at each pulse is sufficiently small, 1000 states can be achieved, as demonstrated in the new Figure 1d. In this specific demonstration, 200 nA/5 ms pulsing was introduced to get an average of 0.3% for $\Delta G/G$ per pulse, generating an overall G_{max}/G_{min} of 30. In the meantime, the conductivity detection limit of the instrument is ~ 0.025% (from specification of Keithley 2460). Therefore, we are confident 1000 states can be achieved on our device. The maximum and minimum resistance values will depend also on the geometry of the device.

We have revised Figure 1d on Page 6 and corresponding main text on Page 10 to reflect this discussion.

Comment: ** low hysteresis is decisive for multi-state operation. I'm a bit surprised that even under current control quite big hysteresis occurs under some conditions, e.g. fig. 2c,d. Any idea why, and how to improve that?*

Response: We ascribe the observed hysteresis during the current controlled gating to the kinetics of proton diffusion in the channel layer. Based on the diffusion coefficient we measured in Figure S13, which drops quickly with the intercalation of proton, the time needed for the proton gradient to equilibrate between the interface of Nafion/WO_3 and the WO_3 bulk is significantly longer with higher hydrogen content. Therefore, with the same sampling period, we had to acquire the non-equilibrated states at higher H content region, leading to asymmetric behavior.

To further reduce the asymmetry, miniaturizing the dimension of the channel material, including reducing thickness and channel length will be most promising. This will significantly reduce the equilibration time needed for the proton to diffuse, revealing the true steady-state conductance. Also, this can reduce the current level needed to achieve similar effect of gating, which is usually accompanied by increased Faradic efficiency. In addition, when operated in smaller H exchange range, the asymmetry can be better than operating with high on/off ratio. For example, the data below shows the low hysteresis when only operated in the extreme case with 1 potentiation/ 1 depression for 100 cycles. Also, as seen in Figure 1d, when the pulse height is 200nA, the inserted hydrogen amount during each pulse is less, and the equilibration is faster, thus giving a more symmetric potentiation/depression behavior even with 1000 pulses.
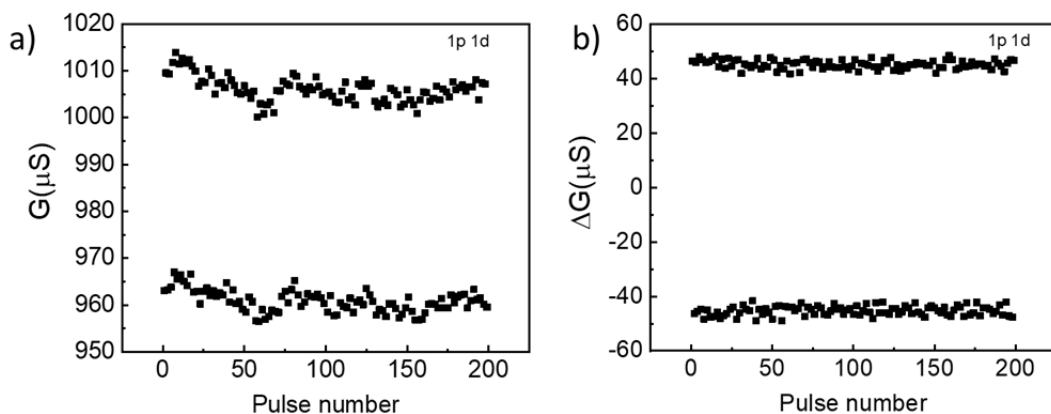
Figure R1(also S16). a) Conductance (G) and b) conductance change (ΔG) with alternating 1 potentiation and 1 depression operation for 100 cycles. Reproducible switching behavior with low hysteresis is evident.

We have added this comment in the main text on Page 11.

Comment: ** According to the reported results, current gating is preferred as operation mode over voltage gating. Please comment if this would lead to any significant complications for*

construction of real devices comprising many such synapse cells (current is more difficult to control than voltage), or how big the chance is to get good performance also in voltage gating

Response: We thank the reviewer for noting the difficulty of constructing constant current source. Indeed, constant current source is less common. In literatures, people have successfully fabricated current source that can supply fast pulse with discrete PFET and NFET. (Tang, J. *et al.* in *2018 IEEE International Electron Devices Meeting (IEDM)*. 13.11.11-13.11.14) This circuit has been used to gate the ECRAM in their demonstration. Therefore, it indeed will need extra circuit elements to achieve the goal, but we believe it is still feasible.
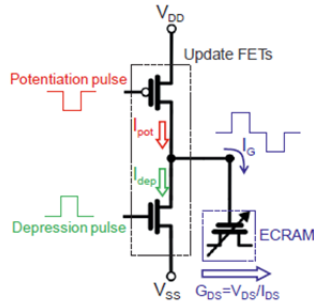

Fig. 7. ECRAM unit cell design for high-speed programming, in which discrete PFET and NFET serve as current source to ECRAM for positive (potentiation) and negative (depression) weight update, respectively.

Figure R2. Realization of current source demonstrated in the literature with fast pulsing capability. (Tang, J. *et al.* in *2018 IEEE International Electron Devices Meeting (IEDM)*. 13.11.11-13.11.14)

We have also performed the test under constant voltage gating. The result and related discussion have been shown in Figure S12. With proper selection of the specific gating voltage, good performance can also be achieved. The only complication during this process is the lack of theoretical guidance to choose the proper gating voltage to get the symmetrical behavior, which could be resolved by calibration curves.

Comment: * *it would be good to comment on the scatter in conductance between a larger number of nominally identical cells (i.e. how reliably can the number of cells be scaled up)*

Response: We believe that reproducibility is a major advantage of our switching mechanism vs the conductive filament mechanism. The main cause of lack of reproducibility of the conducting filament devices is the stochastic nature of the filament formation. In contrast, the protonation mechanism is deterministic and charge controlled. The conductivity of our channel is defined by a bulk material property, which is the hydrogen amount in H_xWO_3. This deterministic approach that uniformly protonates or deprotonates the channel material should give a much more reproducible behavior. Quantification of this as a function of device geometry and material type

will be the scope of our future work. We have added a discussion about this point on Page 5 of the main text.

Comment: ** the cells need humidity in the Nafion layer, and oxygen in- and/or hydrogen out-diffusion must be avoided. Authors report some preliminary encapsulation tests, but longer times than in fig S14 should be reported*

Response: We agree that the encapsulation, and the resulting retention and endurance should be more thoroughly characterized. Currently for our proof-of-concept device, the encapsulation approach is far from being ideal, and rather rudimentary. So any data that we collect with this approach will not represent the true potential of this device for endurance and retention. But we do have longer testing data of the present encapsulated device, that was monitored for 21 hours after a sequence of potentiation cycling as shown in Figure R4 (Figure S15a) below.
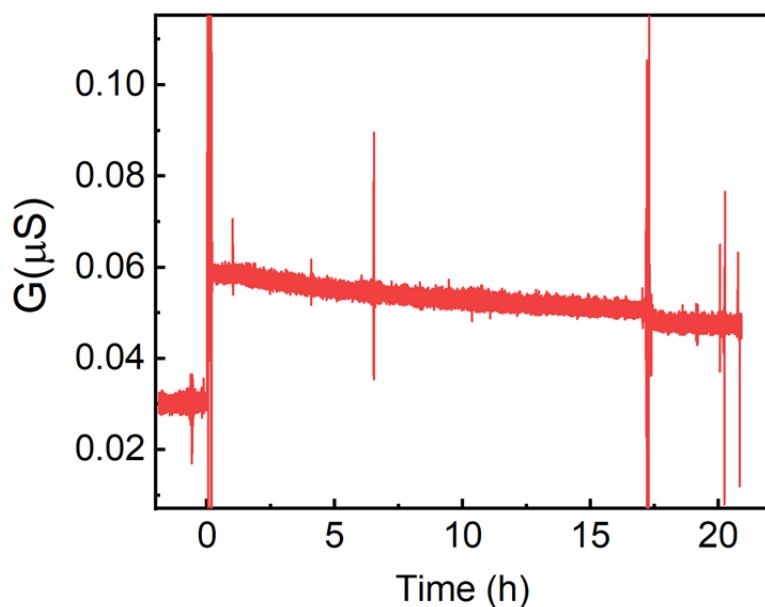

Figure R3. Retention of potentiated state of an encapsulated device over 21 hours. Before t=0, the conductance was 30 nS. At t=0, 10 potentiation pulses doubled the conductance of the channel to 60 nS. The gating circuit was opened and the channel conductance was continuously monitored for 21 hours. The final conductance was 47 nS. To be noted, the encapsulation applied here is still far from ideal, but the result is promising and suggests good retention.

This demonstration is now included in Supplement Figure S15a.

Comment: ** a related issue: Nafion is an acidic polymer. Any long-term degradation in contact with palladium hydride (the hydrogen reservoir) by releasing hydrogen from proton+hydride ions, and incorporation of Pd^{2+} into Nafion for charge compensation?*

Response: Although known and named as Palladium hydride, this is not an ionic hydride. Hydrogen exists as H^0 in Pd metal, forming a solid solution (or an alloy). There is no negatively

charged H$^-$ species, so the reaction with H$^+$ in Nafion is not a concern. Palladium as a noble metal, has high redox potential for Pd^{2+} to form. The reaction of Pd dissolution into Nafion is not very likely within the potential window in which we are operating, which is well below 0.5 V.

Reviewer #2 (Remarks to the Author):

In this manuscript the authors present a very complete work on the development of three-terminal synapses based on proton intercalation in inorganic materials. The work is very complete, as it provides clear information about the fabrication of the devices, complete morphological and electrical characterization, and atomistic modelling. The electrical characteristics measured are impressive, specially the linearity achieved and the controllability of the potentiation and depression processes. The conductance modulation mechanism is clearly identified using "in operando" chemical measurements. Overall, the work provides important insights in its field of research, and the reliability of the findings is higher than in most reports in this field due to the multiple and high quality techniques used. In my opinion, this work is above the level of most others in the field, and for that reason I would like to recommend its publications in Nature Communications.

The only weakness that I see, which the authors should definitely further discuss, is the integration capability of this work:

Comment: *1- First of all, they use devices with channels of 100 um (is that the length or the width?). These devices are very big. Did the authors try to do smaller devices? This is highly recommended in order to observe if the findings also apply to miniaturized devices.*

Response: We agree that the scaling behavior of this device should be thoroughly characterized. The scope of this current paper is to demonstrate the concept and working mechanism of the material and device system. Our present devices were patterned by shadow masks. This limits the size and geometry of the device. However, we are currently working on downscaling the protonic electrochemical synapses with a much smaller footprint by photolithography and an improved layout. This extensive work will be reported in a future publication, and we believe it is out of the scope of our current paper. We hope this is acceptable to the reviewer.

Comment: *2- Moreover, as the authors wrote the word "computing" in the title of their abstract and because the introduction of their paper is discussing about "in memory computing", the authors should discuss what is the potential of their device for computation, which in its current form seems to be unclear to me. The authors should clarify which kind of computation may be done with their device and the path towards such implementation. I do not think it is necessary they demonstrate such computation, but they may reference some works that did such things.*

Response: We thank the reviewer for clarifying the importance of technological background. We have modified the introduction to include specific examples of the applications. Please find the related revision on Page 3 of the main text.

Comment*: 3 – The authors should also indicate which is the advantage and disadvantage of their devices compared to two-terminal resistive switching devices. I think two-terminal resistive switching devices are the most commonly used in most companies, and therefore it seems to me*

that they have most potential to end up being the hardware for such "in memory computing". Therefore, from a technological point of view, the authors should clarify the potential of their work.

Response: We have modified the introduction part to clarify the potential of our work. Please find related revisions on Page 3 and Page 5 of the main text.

Comment: *The work is really good, I really enjoyed reading it, but the authors should provide more practical information about the technological potential of their work. I also recommend to remove the word "computing" from the title; some readers may get too excited when seeing the title and later disappointed when reading the manuscript, as there is not computing in this manuscript. In the future, the authors may try to associate different devices to solve a complex problem. They may even indicate such thing in the conclusions to encourage the community to work in such application.*

Response: We have changed our title to address this concern. The new title reads as follows:

Protonic Solid-State Electrochemical Synapse for Physical Neural Networks

We also modified the conclusion section to state the potential of our device on Page 19 of the manuscript.

Reviewer #3 (Remarks to the Author):

Authors in this work demonstrate a three terminal device based on proton migration. The device shows a great reversibility for analog signal processing under current pulses. They have also performed impressive and careful materials studies both experimentally and theoretically to conclusively reveal the switching mechanism. It is a very interesting and timely work. I strongly recommend it for publication.

I do have some minor comments for the authors to consider.

Comment: 1. *The authors obtained good XAS and XPS results to make comparisons between WO_3 and H_xWO_3, but the exact ratio of O to W of the as-deposited film was not revealed. It would be great if the stoichiometric ratio of O to W is also given in the manuscript. Did author fabricate the WOx film with a non-stoichiometric ratio? How would that affect the performance of the device? How to eliminate the effect of oxygen vacancies migration in WO_x channel?*

Response: Upon deposition by sputtering, we have annealed the films in ambient air. Therefore, we expect them to be (nearly) fully oxidized, WO_3. Based on the XPS spectrum of W4f region and oxidation state analysis below, we conclude that the O:W ratio is at least 2.98.

We used the W4f spectrum analysis to estimate the non-stoichiometry. The W $4f_{7/2}$ peak was deconvoluted into two peaks. The main peak was assigned to be W^{6+} and a very small shoulder peak was assigned to the reduced W^{5+} (for instance due to oxygen vacancies in the as-prepared state). Based on the peak position, these two peaks are ascribed to W^{6+} and W^{5+}, respectively. The relative percentage of these two peaks are 95.5% *vs* 4.5%. This gives an O:W ratio as 2.98. So, we use the notation of WO_3 instead of WO_x throughout our manuscript.

If the O:W ratio were to be low, the initial conductance of the pristine channel will be higher, as a result of mixed oxidation state of W. But the device can still switch, just with a smaller G_{max}/G_{min} ratio.

As to the oxygen vacancy migration in WO_3 channel, we do not expect oxygen to be able to move at room temperature because the field crated between the Source-Drain electrodes is very small. We are using only 0.1 V as reading bias, which is too small to induce oxygen vacancy migration at room temperature.

Comment: *2. The WO_3 film was annealed in air at 450 ℃ for 1 h. Please comment on the concentration and effects of nitrogen in the annealed film. In addition, 450C is higher than 400C, which means this process is not 100% fab compatible yet. Would 400C annealing for a longer time achieve the same effect?*

Response: We examined the N1*s* region of XPS survey spectrum and didn't find any inclusion of N. N_2 is still considered inert at 450 °C toward WO_3.
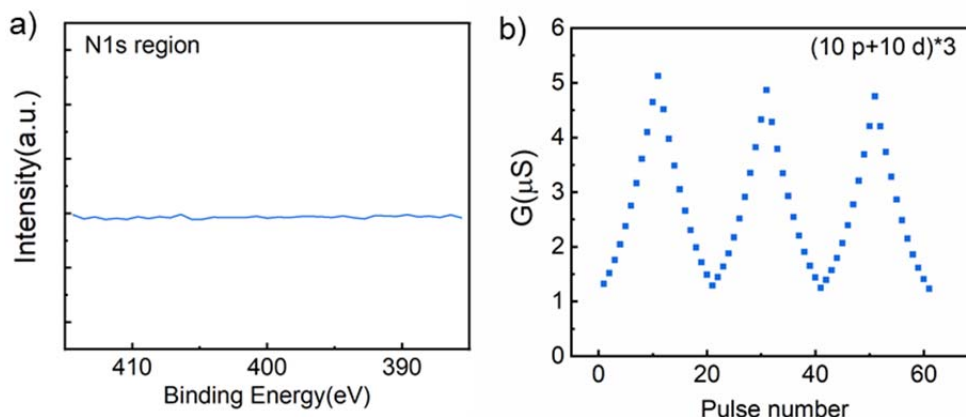

Figure R4. a) N 1s region of XPS survey spectrum obtained from 450°C-WO_3 sample, with no observable N signal. b) Potentiation/depression behavior of 400 °C-WO_3 device. The switching behavior and symmetry is also excellent.

Regarding lower fabrication temperature, we have annealed the WO_3 film at 400 °C for 1h. Although the film is still amorphous, as examined by XRD, the device can deliver the desired switching behavior. We have added the potentiation/depression data of the WO_3 film annealed at 400 °C as Supplementary Figure S5, and shown above in Figure R4(b). We used the 450 °C sample in our main text due to the well-defined crystal structure for the ease of analysis.

As shown above, crystallization of WO_3 is not necessary to induce the proton induced resistive switching behavior. However, if crystalized WO_3 is more desirable, it is possible to obtained crystallized structures at reduced temperatures below 400 °C. Cold sintering, as an example, can accelerate the crystallization of material with lower temperatures (Guo, J. et al. Angew. Chem., Int. Ed. 55, 11457-11461 (2016)). If needed, these modern techniques are available to reduce the processing temperature of such materials and devices, but this also warrants future work to explore.

Comment: *3. Please comment on how to control concentration of hydrogen in Pd, nafion and WO3 during fabrication process? How do we know that H has been incorporated into the Pd films? Can phase/structure of PdHx or Hydrogen forward scattering (HFS) help?*

Response: The introduction of hydrogen into our device was through the chemisorption of H_2 by Pd. The amount can be controlled by the exposure time, hydrogen partial pressure and reaction temperature. Once H is in the Pd, Pd expands, so the XRD can help quantify on how much H is in Pd. Advanced characterization techniques, such as Hydrogen forward scattering or neutron scattering could also give quantitative information of hydrogen concentration.

In our experiments, we have used the open-circuit potential measurement to determine, *in situ*, if the hydrogen absorption has been realized. Before the introduction of hydrogen, the open circuit potential of our device will be defined by the O_2 potential adsorbed on Pd (close to 1.23 V vs. Standard Hydrogen Electrode), which has a positive potential vs. the WO_3/Au electrode. When Hydrogen gas is introduced, H incorporate into Pd to form PdH_x which significantly reduces the potential to nearly 0 V vs. SHE. This makes the open circuit potential of PdH_x negative with respect to WO_3/Au electrode. Based on this observation, we can know if H has been incorporated into Pd or not. We have added this observation into the Experimental methods section on Page 20 of the main text now.

Comment: *4. The relative humidity was 100% during the testing. Does it mean that the devices still somehow rely on water electrolysis? Would any change of the environment humidity affect the proton conductivity of the device? Would the device work well when the test chamber contains hydrogen only? What is the chamber pressure when the devices were tested?*

Response: Lack of water hydrolysis is actually a key difference of our work *vs.* prior work. We do not rely on water electrolysis to supply protons, which is evidenced by the small gating voltage we are using here (<0.5V). To electrolyze the water, the minimum of 1.23 V will necessary to meet the thermodynamic requirement and an additional 0.5~0.7 V is needed to break the kinetic overpotential, even on the best electrocatalyst. So we can confidently rule out the possibility of water electrolysis here. We have added this new discussion on Page 11 of the manuscript.

With the open structure of our demo device, the humidity does have an influence on the proton conductivity of the electrolyte. This is why the reason for measuring in nearly 100% humidity was to maintain the optimum conductivity of the Nafion electrolyte. We indeed have measured the device in dry hydrogen only. There was no difference in terms of switching behavior, but there was an increase of gating voltage at the same gating current. This increase is a result of reduced electrolyte conductivity, which increases the internal iR loss. We have also tested an encapsulated device, which can be done in ambient air, as shown in Figure S6.

The testing chamber for the open structured device was at ambient pressure (~760 torr). The estimated gas composition is Ar (92%), hydrogen (5%), water (3%).

Comment: 5. *In Figure 2b-d, the conductance updating property of the device at low conductance regime shows a better symmetry than that at middle and high conductance regime.*

Why does the symmetry of the conductance updating become worse when the concentration of hydrogen increases? Why there is still an asymmetrical updating in low conductance regime? Since the symmetry of conductance updating with 200 pulses looks better than that with 40 pulses and 100 pulses in low conductance regime, would the symmetry be affected by pulse number?

Response: The reason for the observed hysteresis is more obvious in the high conductance region which has a higher hydrogen concentration. We ascribe the observed hysteresis during the current controlled gating to the kinetics of proton diffusion in the channel layer. The diffusion coefficient we measured in Figure S13, drops quickly with the intercalation of protons. Therefore, the time needed for the proton gradient to equilibrate between the interface of Nafion/WO_3 and the WO_3 bulk is significantly longer with higher hydrogen content. We keep the same sampling period for all protonation regimes, and while this has been sufficient to obtain equilibrated data for the low protonation regime, it is too short for the higher protonation regimes (i.e. the equilibration time is longer than our sampling period). Therefore, we ended up having to acquire the non-equilibrated states at higher protonation regimes, and this leads to an asymmetric behavior.

For the low conductance regime, symmetry is better but some asymmetry is still present, because the amount of H exchanged at each pulse is still considered relatively high, due to the limitation of our current instrumentation. To further reduce the asymmetry, miniaturizing the dimensions of the channel material, reducing the pulse current, and shortening the pulse length will be the most promising. This will significantly reduce the equilibration time needed for the proton to diffuse, revealing the true steady-state conductance. Also, this can reduce the current level needed to achieve similar effect of gating, which is usually accompanied by increased Faradaic efficiency.

We attempt to clarify the symmetry comparison here. The symmetry will be affected by pulse number, but is the opposite than what the reviewer described above. Smaller pulse number means smaller deviation from the equilibrated state of the material, which results in better symmetry. An extreme case is when only 1 potentiation and 1 depression is applied, in which case, we can obtain nearly perfect symmetry, as shown in Figure R5 (also Figure S16) below. With the increase of pulse number, the diffusion factor mentioned above will result in gradual decrease of ΔG per pulse at higher pulse number, resulting in higher asymmetry.
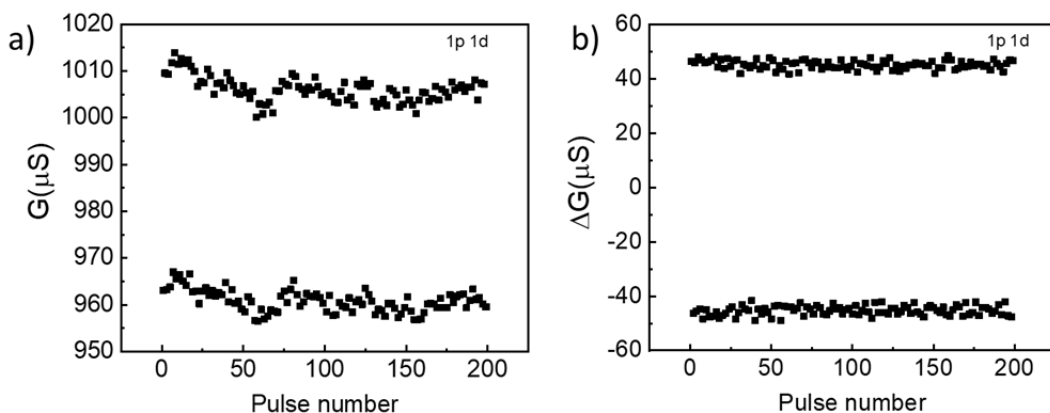
Figure R5 (also S16). a) Conductance (G) and b) conductance change (ΔG) with alternating 1 potentiation and 1 depression operation for 100 cycles. Symmetrical ΔG of potentiation and depression is observed.

Comment: 6. *In Figure 3b, is there a plausible explanation for that the high resistive state of the device becomes more insulative and low resistive state of the device becomes more conductive after large amounts of cycling?*

Response: First, we want to note the change of G_{max} and G_{min} are relatively small in Figure 3b. This trend is not universal to all devices. This phenomenon could be a result of increased Faradaic efficiency during the cycling when the irreversible side reactions are gradually consumed. So, the same level of current can lead to slightly higher amount of actual hydrogen intercalation.

Comment: *7. on Page 7, there is a typo, "As demonstrated in Figure 1a, over seven orders ..." should be Figure 2a.*

Response: We have made the correction (on Page 8 now) and examined the full manuscript again to make sure the consistency.

Comment: *8. on Page 9 about Figure 2a "...after 100 positive gating pulses, the conductance of the channel increased from 1 μS to 22 μS, ..." it's a bit confusing here, what is the pulsing sequence, from 100 down counting to 1 in Figure 2b? please use arrows to label them in the figure.*

Response: We have added arrows indicating the direction of operation in Figure 2b-d for clarification.
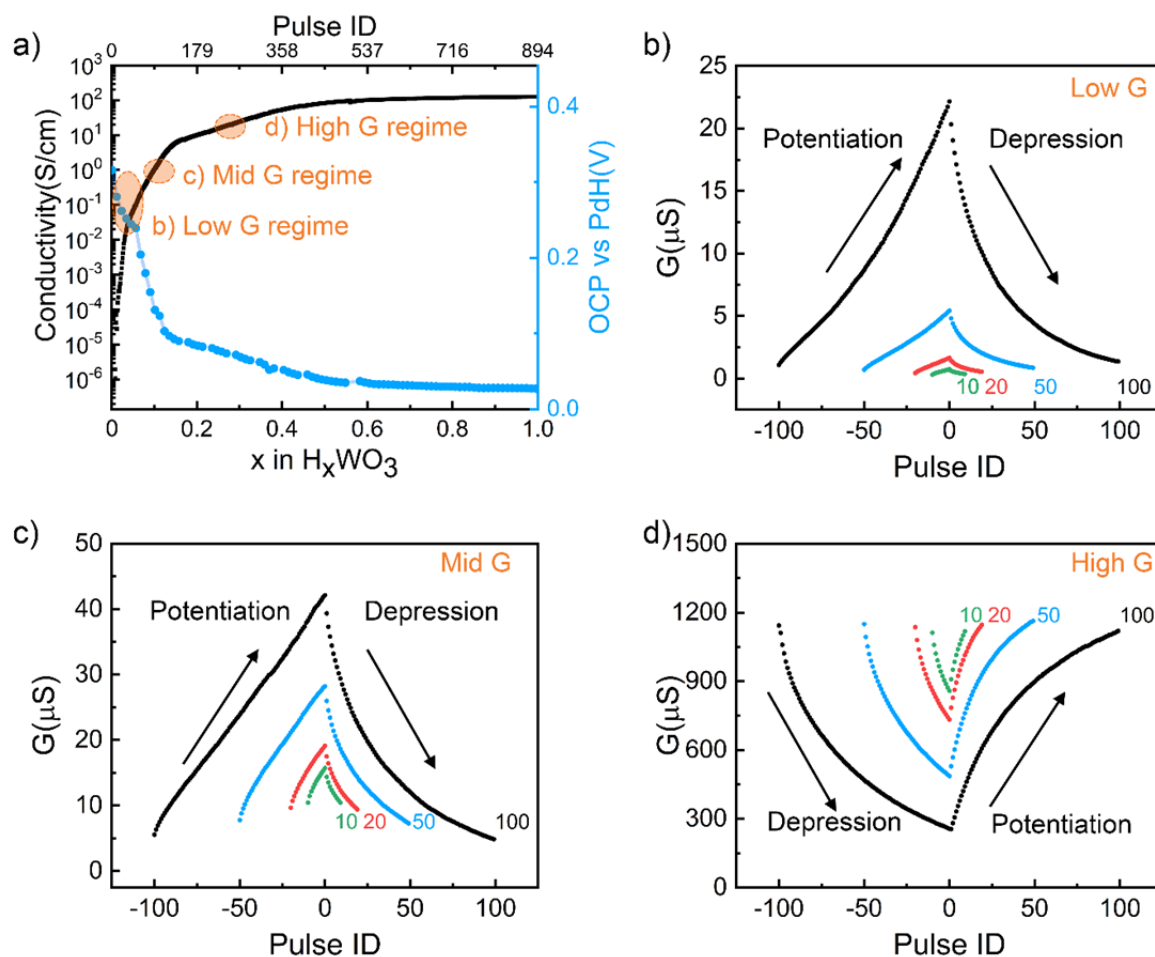
Comment: 9. *The specific pulse height-width that was used to achieve each conductance regime (low, medium and high) should be clearly stated in the caption of Figure 2 or the main text.*

Response: We have added this information to the caption of Figure 2 to indicate the pulses needed to modulate the conductance to the desired level.

Comment: *10. Endurance to the level of million has not been demonstrated (and not really expected for this paper as well). Is that due to testing time or failure? Please comment on possible failure mode?*

Response: We do have limitations at the current stage of development for cycling test. With the present pulse height/width, our testing protocol requires 1s for each cycle for stable conductance readout, 1 million cycles with 100p/100d will require 6 years for test. We're in the process of setting up to use nA and ns pulse regime, and examining the endurance in that regime will be more feasible. Regarding the failure mode, the devices do fail after prolonged operation. The most common failure mode is the increase of internal resistance as a result of Nafion electrolyte degradation, due to the loss of water content to the environment. A better electrolyte choice that do not rely on hydration to conduct proton is desired, and we're also working on this. Another major reason for the failure of encapsulated device is the depletion of active hydrogen in the

11

system. As we discussed in *Supplementary Discussion 2*, the ingression of oxygen, diffusion of hydrogen, and less than 100% Faradic efficiency will all contribute to this aspect. However, our present encapsulation is far from ideal, and this behavior does not represent the true potential of the device. The last failure mode is the degradation of electrode material. After the hydrogen is absorbed by Pd, there will be a relatively large volume expansion (as PdH_x is an alloying reaction, not intercalation reaction), upon repeated cycling, Pd layer may detach from Nafion surface. This requires improved adhesion layer at Nafion/Pd interface or other material choice as hydrogen reservoir other than Pd metal.

We have expanded the discussion to reflect on the potential failure modes of these devices on Page 12-13 in the main text.

Comment: *11. As the author mentioned, "When the external circuit is cut off (gate is open circuit), the electronic insulating nature of the electrolyte prevents the back flow of electrons, and consequently that of protons too." Therefore, a two-terminal threshold volatile switch was used to provide both selector and threshold functions for programming (e.g. NatMat 16, 396, 2017), without which an array of such devices may only be programmed column-wise or row-wise (not randomly and individually programming a device in the array during learning). Will the device studied here also need such as threshold switch on the gate?*

Response: For the current device configuration, there is a non-zero open circuit potential (OCP) change after the gating, so the selector is needed to program individual synapse in an array, as demonstrated by recent publication in *Science* **364,** 570-574 (2019), and to avoid cross-talk of individual synapses when not gating. We have added notes on Page 12 in the manuscript to reflect this point.

If the device possesses OCP = 0 V or the change of OCP after gating remain the same, there is no need for the two-terminal selector to program each individual synapse. The small OCP change after gating has been successfully demonstrated in our work as shown in Figure 2a, for the x= 0.6~1 region. But it is still far from desirable and the corresponding conductivity change in this region is relatively small. Further work is on-going in our lab to achieve the true zero-OCP change during the gating.

Comment: *12. A constant current source (compared to a voltage source) is usually not preferred in real circuits due to various reasons.*

Response: We are aware of this challenge and have performed the test under constant voltage gating, too. The result and related discussion are shown in Figure S12. With proper selection of the specific gating voltage, good performance can also be achieved with our device.

In the literature, researchers have successfully fabricated current source that can supply fast pulse with discrete PFET and NFET. (Tang, J. *et al.* in *2018 IEEE International Electron Devices Meeting (IEDM).* 13.11.11-13.11.14) This circuit has been used to gate the ECRAM in their demonstration. Therefore, it indeed will need extra circuit elements to achieve the goal, but we believe it is still reasonable.
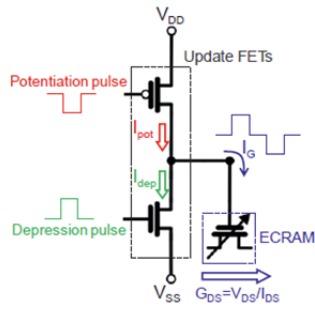
Fig. 7. ECRAM unit cell design for high-speed programming, in which discrete PFET and NFET serve as current source to ECRAM for positive (potentiation) and negative (depression) weight update, respectively.

Figure R6. Realization of current source demonstrated in literature with fast pulsing capability. (Tang, J. *et al.* in *2018 IEEE International Electron Devices Meeting (IEDM)*. 13.11.11-13.11.14)

REVIEWERS' COMMENTS:

Reviewer #1 (Remarks to the Author):

the revision answers my questions adequately, paper can be published now

Reviewer #2 (Remarks to the Author):

The authors have made a good revision of my previous comments, and I think the manuscript reaches the level of other papers published in Nature Communications in this field of research. I believe publishing this manuscript is a good choice.

Just one minor point. I recommended the authors to remove the word "computing" form the title and they did. But they replaced by "neural network". I think this manuscript demonstrates in a very clear way that the devices exhibit some synaptic behaviors, but they do not go beyond that. I think the authors should still modify the title and remove any work that points to association of devices (such as computing or neural network), otherwise the readers is going to be confused and overall gives the impression that the authors try to oversell their work. The work is already excellent in its field, such overselling is not necessary. So, better to change the title and make it more descriptive of the content.

Other than this, the paper is excellent. Congratulations to the authors for this excellent achievement.

Reviewer #3 (Remarks to the Author):

The authors have addressed my questions satisfactorily in the revision, which is recommended for publication as is now.

REVIEWERS' COMMENTS:

Reviewer #1 (Remarks to the Author):

the revision answers my questions adequately, paper can be published now

Response: We are pleased to find the reviewer is satisfied with our revision and thank the reviewer for the support.

Reviewer #2 (Remarks to the Author):

The authors have made a good revision of my previous comments, and I think the manuscript reaches the level of other papers published in Nature Communications in this field of research. I believe publishing this manuscript is a good choice.

Just one minor point. I recommended the authors to remove the word "computing" form the title and they did. But they replaced by "neural network". I think this manuscript demonstrates in a very clear way that the devices exhibit some synaptic behaviors, but they do not go beyond that. I think the authors should still modify the title and remove any work that points to association of devices (such as computing or neural network), otherwise the readers is going to be confused and overall gives the impression that the authors try to oversell their work. The work is already excellent in its field, such overselling is not necessary. So, better to change the title and make it more descriptive of the content.

Other than this, the paper is excellent. Congratulations to the authors for this excellent achievement.

Response: We appreciate the review's support of our paper, constructive review, and suggestion to modify the title again. We revised our original title per this reviewer's comment, and included the "physical neural network" in the title to indicate the targeted application field of our artificial synapse. This clarification of potential application is also in line with the reviewers' recommendation in the first round of review, *"The authors should clarify which kind of computation may be done with their device and the path towards such implementation.".* We believe this will help to distinguish our study from the studies on the biological synapses, and also from biological applications of artificial synapses (neuroprosthetics). The presence of "physical neural networks" helps to better reach the targeted readership of this article. We hope you can support our preference in keeping the title as is now.

Reviewer #3 (Remarks to the Author):

The authors have addressed my questions satisfactorily in the revision, which is recommended for publication as is now.

Response: We are pleased to find the reviewer is satisfied with our revision and thank the reviewer for the support.